DETERMINATION OF KINETIC CONSTANTS AND THERMAL MODELING OF PYROLYSIS OF PALM OIL MILL SOLID WASTES

by

JESUS ALBERTO GARCIA-NUÑEZ

(Under the Direction of Keshav C. Das)

ABSTRACT

Empty fruit bunches, fiber, and shell are the main solid residues produced during oil extraction process from oil palm (*Elaeis guineensis Jacq.)*. These biomass were subject to thermogravimetric (TG) and differential scanning calorimetry (DSC) analyses to determine the kinetic parameters activation energy (*E*), frequency factor (*A*), and reaction order (*n*). The shapes of TG and DSC curves were used to identify the number of thermal degradation steps for these materials. Thermal degradation kinetic parameters were obtained for each of the steps identified. TG and DSC curves were used in a thermal model for predicting char production during the pyrolysis of shell in an indirectly heated continuous reactor. The model consisted in establishing a set of equations that allows predicting temperatures and residual mass in different parts of the reactor. Using the software Engineering Equation Solver (EES), the model was capable of calculating char yield with a 1.12% error compared to the measured values. The model was used to predict char production on fiber and EFB at different temperatures.

INDEX WORDS: Oil palm biomass, pyrolysis, thermal analyses, TG, DSC, empty fruit bunches (EFB), oil palm fiber, oil palm shell, thermal model

DETERMINATION OF KINETIC CONSTANTS AND THERMAL MODELING OF PYROLYSIS OF PALM OIL MILL SOLID WASTES

by

JESUS ALBERTO GARCIA-NUÑEZ

B.S., University of Valley, Colombia, 1991

A Thesis Submitted to the Graduate Faculty of The University of Georgia in Partial Fulfillment of the Requirements for the Degree

MASTER OF SCIENCE

ATHENS, GEORGIA

2005

DETERMINATION OF KINETIC CONSTANTS AND THERMAL MODELING OF PYROLYSIS OF PALM OIL MILL SOLID WASTES

by

JESUS ALBERTO GARCIA-NUÑEZ

Major Professor:	Keshav. C. Das
Committee:	Mark A. Eiteman Thomas T. Adams Thomas M Lawrence

Electronic Version Approved:

Maureen Grasso
Dean of the Graduate School
The University of Georgia
December 2005

DEDICATION

To Luz Aida, Gabriel Alberto, and José Fernando with all my love.

To my parents, brothers, and sisters.

To my mother in law, my sister in law, and brothers in law.

ACKNOWLEDGMENTS

I would like to express my appreciation to everyone who helped me to finish my master of science. I am very thankful to:

- Fulbright and Colciencias for the scholarship they gave me to pursue my studies in US.
- Cenipalma for the opportunity to do my master. Special thanks to Dr. Pedro Leon Gomez for his support and encouragement to start and finish my postgraduate studies.
- My major professor, K.C. Das for his support, encouragement, and guidance throughout this project.
- My committee members: Drs. Tom Lawrence, Mark Eiteman, and Tom Adams for their advices and suggestions during this project.
- Dr. Manuel García for his contribution to the project and for his professional and personal advices.
- Ms. Mary Sue Brewer who helps us during the thermogravimetric and differential scanning calorimetric analyses.
- Pat Harrell for his work during the construction of the pyrolyser.
- My colleagues, specially, Ravi, Brenda, Erik, Praveen, Shiying Lu and Yihui, and the entire graduate club for made me feel at home.
- My neighbors on campus for bringing the ideal world to a small place.

TABLE OF CONTENTS

Page

LIST OF TABLES

Page

LIST OF FIGURES

Page

CHAPTER 1

INTRODUCTION AND LITERATURE REVIEW

Pyrolysis of biomass is the thermal degradation of the organic matrix in the absence of oxygen to obtain charcoal, bio-oil, and gases as products [1]. Pyrolysis has been used since ancient times not only for the production of charcoal but also for recovering distillation-products. At the end of the 19^{th} century and the beginning of the 20^{th} wood distillation was a profitable industry for producing, acetic acid, acetone, and methyl alcohol among other products [2, 3]. With the advent of the petroleum industry, pyrolysis declined as a means of production of chemical compounds. Nowadays, because of energy and environmental concerns, pyrolysis of biomass is receiving increasing attention for production of pyrolytic liquid fuels, gaseous fuels, organic chemicals, and activated carbon [4]. In a review paper, Yaman [1] reported more than one hundred biomass species whose pyrolysis behavior has been studied.

The palm oil industry is an important agricultural business in developing countries. Among vegetable oils, palm oil is the second largest oil produced worldwide surpassed only by soybean oil. In 2000 palm oil production was 21.71 million tonnes and soybean oil production was 25.21 millions tonnes worldwide [5]. Palm oil and its fractions are used mainly for food products such as cooking oils, bakery products, margarine and, shortening [5]. Non-edible uses of palm oil include the production of oleochemical compounds such as sulfonated methyl esters, polyols, and polyurethanes [5].

The industrial process of extracting palm oil consists of the following steps [5]: Fresh fruit bunches (FFB), harvested from the field are transported to the palm oil mill where they are

sterilized for 1 h at 3 kg $(cm^2)^{-1}$ steam pressure in a cylindrical vessel. The main goal of this step is to prevent the increase of free fatty acid (FFA) and to loosen the fruit on the bunch to facilitate stripping. The separation of the fruits from the bunches is done in a horizontal drum that allows the fruit to fall through, while the empty fruit bunches (EFB) go out from the end of the drum. Fruit from the stripper is carried by conveyor belt to the digestion section. The digester, a vertical cylinder with rotating beater arms, macerates the fruit, loosening the pulp from the nut. The mass of nuts and fruits is heated in the digester before passing into a screw press where the oil is squeezed out. The digested mixture of fiber, oil, and nuts is forced through a perforated press cylinder by the rotation of the screw, or counter-rotating screws in the double screw press. Adjustable cones restrict the exit of the mass, so that pressure increases in the press cylinder. The crude oil (oil, water and other 'non-oil solids') goes out through the perforated cylinder to a small settling tank. The cake (nuts, and moist fiber with some residual oil coming from the presses) is carried to the kernel section.

The oil/water mixture is fed into the middle of a continuous setting tank, where oil is steadily removed from the top and sludge is removed from the bottom. The oil and waste fractions are then centrifuged. The oil is dried using vapor extraction units or vacuum dryers to prevent FFA formation by autocatalytic hydrolysis. The dry oil is storage in welded tanks. In the kernel section the cake, which comes out from the presses, is separated into nuts and fiber. The fibers are used in boilers to produce stream for the process and the nuts are broken to obtain shell and kernel, which is the second marketable product from a palm oil mill.

The amounts of palm oil and kernel produced are around 20 and 4.5 % (wet weight basis) of fresh fruit bunches (FFB). The main solid residues produced at a palm oil mill (POM) are empty fruit bunches (20% of FFB), fiber (13% of FFB), and shell (4% of FFB). A single POM

of average capacity (60 tonne FFB/h) can produce as much as 100,000 tonnes of solid residues annually. The conventional use of EFB as a soil conditioner is not attractive because of the high cost of transportation. Fibers are typically used as fuel in boilers that produce steam, and shells are used as a low value surface cover in the plantation internal roads. After using all the fiber required to produce steam, a typical POM still has around 30% of available biomass as FFB that could be used in other higher value beneficial uses.

One of the obstacles to widespread use of pyrolysis technologies is the availability, uniformity and cost of biomass [6-8]. In the case of the oil palm industry, the potential use of this free biomass located at a single point, and the synergies of having a pyrolysis unit coupled with existing infrastructure represents an opportunity for improving the process in a palm oil mill.

In order to know how if a specific biomass can be used in a thermal conversion process, it is necessary to characterize the biomass for its chemical properties and thermal behavior. Thermogravimetric analysis (TG) and differential scanning calorimetry (DSC) are two of the most commonly used methods to study degradation and heat flows during pyrolysis of biomass [1, 9]. TG records the weight loss when a sample is heated in an oxygen free atmosphere. Differential thermogravimetric data (DTG) obtained by differentiating TG data are commonly used to estimate thermal degradation kinetic parameters such as activation energy (E), frequency factor (A) and reaction order (n). DSC data can provide a more complete picture of biomass thermal degradation mechanisms by including transformations that do not produce a measurable mass loss [10, 11]. DSC measures the amount of heat energy absorbed or released by a sample as it is heated, cooled, or held at a constant temperature [9-11]. Combined thermal analysis using information from both DSC and TG analyses has been used in studying biomass pyrolysis

process [12-14]. However no reports have been found to describe the process of obtaining kinetic constants using combined DSC/TG analyses which provides higher accuracy in identifying initial and final temperatures corresponding to individual transformation steps.

Little information about the kinetic constants and pyrolysis of palm oil mill biomass has been reported. Guo and Lua [15, 16] reported the kinetic constants for shell and fiber for different samples sizes and heating rates using TG analyses. However, the kinetic constants for EFB have not been yet reported in the literature. The same authors [17, 18] reported some works to obtain phenolic compounds from the bio-oil and activated carbon from the char. In addition, no reports have been found in modeling biomass pyrolysis using DSC/TG techniques combined with heat transfer equations in flow continuous reactor.

One of the goals of this research is to determine the kinetic parameters of the three solid biomass components from a palm oil mill using TG/DSC analyses. The second goal is to study the effect of the chemical composition of these residues on their thermal degradation. These two goals are achieved in Chapter 2 of this report. The last goal on this work is to implement a pyrolysis thermal model which includes DSC/TG data combined with energy and mass transfer equations in a continuous reactor. This goal is achieved in Chapter 3.

REFERENCES

1. Yaman, S., *Pyrolysis of biomass to produce fuels and chemical feedstocks.* Energy Conversion and Management, 2004. **42**: p. 651 - 671.
2. Klar, M., *The Technology of Wood Destillation*. Second ed. 1925, London: Chapman & Hall Ltda. 496.

3. Lédé, J., M. Ferrer, and F. Broust, *Fast Pyrogasification and/or Pyroliquefaction of Biomass in a Cyclone Reactor*, in *Pyrolysis and Gasification of Biomass and Waste*, A.V. Bridgwater, Editor. 2003, CPL Press: Birmingham. UK. p. 706.
4. Vasalos, I.A., M.C. Samolada, and G.E. Achladas, *Biomass Pyrolysis for Maximizing Phenolic Liquids*, in *Research in thermochemical biomass conversion*, E.a. science, Editor. 1988, Elsevier Science Publishers ltda.: Essex, England. p. 241 -263.
5. Corley, R.H.V. and P.B. Tinker, *The oil palm*. 4th ed. World agriculture series. 2003, Oxford ; Malden, MA: Blackwell Science. xxviii, 562 , [16] of plates.
6. Grassi, G., *The European R&D Programme*, in *Research in Thermochemical Biomass Conversion*, A.V. Bridgwater and J.L. Kuester, Editors. 1988, Elsevier Science Publishers LTDA: New York, US.
7. Sun, L., M. Xu, and R.F. Sun, *Behaviour of Corn Stalk in an Indirectly Heated Pyrolysis Reactor*, in *Pyrolysis and Gasification of Biomass and Waste*, A.V. Bridgwater, Editor. 2003, CPL, Press: Birmingham, UK. p. 706.
8. Wan, E.I. and M.D. Fraser, *Economic Potential of Producing Liquid Tranportation Fuels From Biomass*, in *Research in Thermochemical Biomass Conversion*, A.V. Bridgwater and J.L. Kuester, Editors. 1988, Elsevier Science Publishers LTDA: New York, US.
9. Gaur, S. and T.B. Reed, *Thermal Data for Natural and Synthetic Fuels.* 1998, New York: Marcel Dekker. 259.
10. Laye, P.G., *Differential Thermal Analysis and Differential Scanning Calorimetry*, in *Principles of Thermal Analysis and Calorimetry.*, P.J. Haines, Editor. 2002, The Royal Society of Chemistry: Cambridge, UK. p. 10 - 54.

11. Heal, G.R., *Thermogravimetry and Derivative Thermogravimetry*, in *Principles of Thermal Analysis and Calorimetry.*, P.J. Haines, Editor. 2002, The Royal Society of Chemistry: Cambridge, UK. p. 10 - 54.

12. Statheropoulos, M., et al., *Thermal degradation of Pinus halepensis pine-needles using various analytical methods.* Journal of Analytical and Applied Pyrolysis, 1997. **43**: p. 115 - 123.

13. Arvelakis, S., et al., *Prediction of the behaviour of biomass ash in fluidized bed combustors and gasifiers.* Journal of Thermal Analysis and Calorimetry, 1999. **56**: p. 1271 - 1278.

14. Stenseng, M., A. Jenses, and K. Dam-Johansen, *Investigation of biomass pyrolysis by thermogravimetric analysis and differential scanning calorimetry.* Journal of Analytical and Applied Pyrolysis, 2001. **58-59**: p. 765 - 780.

15. Guo, J. and A.C. Lua, *Kinetic study on pyrloysis of extracted oil palm fiber. Isothermal and non-isothermal conditions.* Journal of Thermal Analysis and Calorimetry, 2000. **59**: p. 763-774.

16. Guo, J. and A.C. Lua, *Kinetic study on pyrolytic process of oil-palm solid waste using two-step consecutive reaction model.* Biomass and Bioenergy, 2001. **20**: p. 223-233.

17. Guo, J. and A.C. Lua, *Preparation and characterization of adsorbents from oil palm fruit solid wastes.* Journal of Oil Palm Research, 2000. **12**(1): p. 64 - 70.

18. Guo, J. and A.C. Lua, *Preparation of activated carbons from oil-palm-stone chars by microwave-induced carbon dioxide activation.* Carbon, 2000. **38**: p. 1985 - 1993.

CHAPTER 2

DETERMINATION OF KINETIC PARAMETERS OF THERMAL DEGRADATION OF PALM OIL MILL BIOMASS USING THERMOGRAVIMETRIC ANALYSIS AND DIFFERENTIAL SCANNING CALORIMETRY[1]

[1] J.A. García-Núñez, M. García-Pérez, and K.C. Das. 2005. To be submitted to *Biomass and Bioenergy*

Abstract

Empty fruit bunches (EFB), fiber, and shell are the main solid residues produced during extraction of oil from oil palm (*Elaeis guineensis Jacq.)*. Thermogravimetric (TG) and Differential Scanning Calorimetry (DSC) analyses were carried out on samples of empty fruit bunch (EFB), fiber, and shell as received and after solvent extraction. The shapes of TG and DSC curves were used to identify the various degradation steps for these materials. Thermal degradation kinetic parameters (activation energy (*E*), frequency factor (*A*) and reaction order (*n*)) were obtained for each of the steps identified. Presence of extractives and ash had a strong effect on the thermal behavior of EFB. Chemical compositions of extractive free samples were estimated using a thermal kinetic description based on three independent reaction models. The composition obtained by this method did not agree with that determined by conventional analytical techniques.

Keywords: Oil palm biomass, pyrolysis, thermal analysis, TG, DSC, empty fruit bunches (EFB), oil palm fiber, oil palm shell.

1. Introduction

The palm oil industry is an important agricultural business in countries such as Malaysia, Indonesia, Thailand, Nigeria and Colombia. Palm oil and its fractions are used mainly for food products such as cooking oils, bakery products, margarine and, shortening [1]. Non-edible uses

of palm oil include the production of oleochemical compounds such as sulfonated methyl esters, polyols, and polyurethanes [1]. Among vegetable oils, palm oil is the second largest oil produced worldwide surpassed only by soybean oil. In 2000 palm oil production was 21.71 million tonnes and soybean oil production was 25.21 millions tonnes worldwide [1].

The main products of a palm oil mill (POM) are oil and kernel in amounts around 20 and 4.5 % (wet weight basis) of fresh fruit bunches (FFB). The main solid residues produced at a POM are empty fruit bunches (20% of FFB), fiber (13% of FFB), and shell (4% of FFB). A single POM of average capacity (60 tonne FFB/h) can annually produce 54,000 tonnes of empty fruit bunches (EFB), 35,100 tonnes of fiber, and 10,800 tonnes of shells. The conventional use of EFB as a soil conditioner is not attractive because of the high cost of transportation. Fibers are used as fuel in boilers that produce steam, and shells are used as surface cover in the plantation internal roads. After using all the fiber required to produce steam, a typical POM still has about 30% of FFB as biomass available that could be used in other higher value beneficial uses. The potential use of this free biomass located at a single point, and the synergies of having a pyrolysis unit coupled with existing infrastructure represents an opportunity for improving the process in a palm oil mill.

Pyrolysis, the thermal degradation of biomass in the absence of an oxidizing agent, is an important thermochemical process because it is both an independent process used to transform biomass to products, and is also the first step in gasification and combustion [2-5]. The yield of pyrolysis products (char, bio-oil and gases) depend on the type of feedstock used and on process conditions such as heating rate, maximum temperature, and residence time, among others [6-8]. Pyrolysis of biomass has been extensively reported with more than one hundred biomass species been studied so far [4]. However, most of the studied feedstocks are woody biomass. Few

reports were found about the pyrolysis of POM biomass wastes [5, 9-11]. During the past 15 years, biomass conversion is moving forward to find high valued products from the bio-oil [6-8].

Thermogravimetric analysis (TG) and differential scanning calorimetry (DSC) are two of the most commonly used methods to study degradation and heat flows during pyrolysis of biomass [4, 12]. Differential thermogravimetric data (DTG) obtained from TG analysis are commonly used to estimate thermal degradation kinetic parameters such as activation energy (*E*), frequency factor (*A*) and reaction order (*n*). DSC data can provide a more complete picture of biomass thermal degradation mechanisms by including transformations that do not produce a measurable mass loss [13, 14]. DSC measures the amount of heat energy absorbed or released by a sample as it is heated, cooled, or held at a constant temperature [12-14]. DSC/TG techniques has been used in studying *Pinus halepensis* (forest species in the Mediterranean) [15], olive residue [16], and cellulose and wheat straw [17].

Very little information on the kinetics of oil palm biomass degradation has been reported in the literature [2, 18]. Kinetic constants of fiber measured at heating rates of 5 to 30°C min^{-1} indicates that at larger heating rates both the activation energy and the frequency factor decreases [18]. The TG analysis was divided into two temperature zones. A low temperature zone (from 133 to 352°C with a peak at 293°C), for a constant heating rate (10 °C min^{-1}) and different sample particle sizes (from < 0.3 mm to 1.0 – 2.0 mm), the activation energy was found to be 98.2 to 142.8 kJ mol^{-1}. The frequency factor in this range was found to be in the range of 3.06 x 10^7 to 1.21 x 10^8 s^{-1}. In the second high temperature zone (from 352 to 548°C with a peak at 415 °C) activation energy and frequency factor were found to be 153.4 to 189.3 kJ mol^{-1} and from 1.09 x 10^{13} to 2.67 x 10^{14} s^{-1}, respectively [18]. In this work, the first step is identified as

corresponding to hemicellulose decomposition while the second step corresponds to cellulose decomposition.

Oil palm shell was also studied to determine the effect of material particle size (0.3- 0.5, 0.5-1, 1-2, and 2-2.8 mm) and heating rates (5 – 30°C min^{-1}) on the values of the kinetic constants [2]. Using a one-step kinetic model the order of reaction was found to be approximately 1.0, the activation energy was between 54.1 and 55.3 kJ mol^{-1} and the frequency factor was between 7.54 x 10^3 and 1.36 x 10^4 s^{-1}. When a two-step kinetic model (high and low temperature zone) was used, a better fitting model was obtained. In the low temperature regime, activation energy was found to be between 106.4 and 126.5 kJ mol^{-1} while the frequency factor ranged between 4.02 x 10^7 and 8.65 x 10^8 s^{-1}. For the high temperature regime, the activation energy ranged between 169.0 and 161.4 kJ mol^{-1} and the frequency factor ranged between 1.04 x 10^{13} and 8.50 x 10^{12} s^{-1}.

No reports have been found in the literature that describe the process of obtaining kinetic parameters using TG analysis combined DTG and DSC data, which can improve the accuracy of identifying initial and final temperatures corresponding to each transformation step. In addition, although EFB is the principal byproduct stream within POM, EFB kinetic parameters have not been reported in the literature. The main objective of this paper is to report on the thermal degradation of oil palm mill solid wastes using TG and DSC analyses. DSC measurements are used in the identification of the range of temperatures associated to each of the pyrolysis reaction steps.

2. Materials and Methods

2.1 Biomass acquisition and preparation

Oil palm shells, empty fruit bunches (EFB), and fibers were obtained from Manuelita, a POM located in Meta, Colombia. The samples were shipped from Colombia to Athens, Georgia, USA where they were stored at 4°C until further use. The process of oil palm extraction causes small amounts of kernel and fiber to be present as contaminants in the final raw shell fraction and vice versa. These fractions were manually removed to obtain clean fractions of shell and fiber that were used to carry out the experiments. The clean samples of shell, fiber and EFB were dried at 105 °C for 24 h. Particles larger than 2 mm were grounded using a Thomas Scientific laboratory grinder. A Tecator sample mill (Cyclotec 1093) was used to obtain particles sizes smaller than 2 mm. Broken shells from the Thomas Scientific grinder were sieved to obtain particles sizes between 2 and 2.8 mm. Shell, fiber, and EFB from the Tecator mill were sieved to obtain particles with diameter smaller than 0.5 mm.

2.2 Elemental and Chemical Analyses

C, N, and S content in the biomass were measured using a Leco CNS 2000 analyzer. Ash was measured following the ASTM D 3174 method. Metals content in the ash were determined using Inductively Coupled Plasma-Mass Spectroscopy (Perkin-Elmer Elan 6000 ICP-MS equipment) on an ash sample previously digested using mineral acids. The content of lignin, cellulose and hemicellulose was measured on defatted samples by using an Ankom$^{200/220}$ fiber analyzer.

Extractives were separated using a modify version of the ASTM D 1105-96 (re-approved 2001) standard method. Approximately 7.5 g of sample with particle size less than 0.5 mm was

extracted over 4 hours in a Soxhlet apparatus with pre-distilled ethanol-toluene mixture at a volume ratio of 1:2. This step was followed by a similar extraction using methanol and another extraction using water.

2.3 Thermogravimetric and DSC analyses

A TG Mettler Toledo TGA/SDTA851e was used for the thermogravimetric tests. For shell particle size between 2 and 2.8 mm, the samples size varied from 4 to 36 mg. For samples with particle size less than 0.5 mm, the sample size was around 19 mg. Nitrogen at a constant flow rate of 50 cm^3 min^{-1} was used to allow inert atmosphere during the pyrolysis and to remove gaseous and condensable products resulting from pyrolysis. Biomass samples were heated from 25 to 600 °C or 800°C at a constant heating rate of 10 °C min^{-1}.

DSC measurements were carried out in a Mettler Toledo DSC821e. The sample size used was approximately 13 mg. Nitrogen flow rate used was 100 cm^3 min^{-1}. Samples were heated from 25 to 600 °C or 800°C at a constant heating rate of 10 °C min^{-1}. To allow gases to escape freely, the lid of the aluminum crucible (40 μL) was drilled with two small holes. The equipment was calibrated using indium standards obtained from the manufacturer.

3 Results and Discussion

3.1 General Biomass Characterization

The raw shell sample as received had 95.7 mass % of shell and 4.3 mass % of kernel and fiber as contamination. The raw fiber sample contained 0.3 mass % of kernel, 0.7 mass % of whole nuts, and 0.4 mass % of broken shell. The moisture content of the raw shell, EFB, and fiber was found to be 12.30, 68.97, and 38.12 %, respectively. Probably due to the high moisture

content in EFB, there were some fungi in the sample when it was received. After drying and grinding, the samples gained moisture to equilibrate with the moisture content of air. In all cases the moisture content of the materials was less than 6 mass % (Table 2.1).

The composition of C, N and S, ash and volatiles is presented in Table 2.1. It is interesting to note the relatively high contents of ash present in the EFB (7.9 mass %) and fibers (8.44 mass %). Table 2.2 shows the content of metals present in the ash. EFB had the highest concentration of K with 2.2 mass % compared with 0.5 and 0.1 mass % for fiber and shell, respectively. Concentrations of Al, Fe, Ni, Cu, and Pb were higher in the fine shell sample (< 0.5 mm) than the larger size shell (> 2 mm) (2.2). EFB also showed the highest concentration of Na, while fiber had the highest concentrations of Mg, Al, Ca, and Fe. Some of these metals are known to act as catalysts modifying the thermal degradation of biomass constituents.

The chemical composition of samples is presented in Table 2.3. The lignin content in shell was found to be 49.59 %, a value significantly higher than in fiber or EFB. Gaur and Reed [12] note that lignin forms about 30% by weight of typical biomass samples. Few biomass materials have lignin contents as high as shell. Some reported examples are cotton coconut shell [19] with 48.7 mass % of lignin and olive stone with 50.4 mass % [20]. Lignin is the main precursor to char formation and is responsible for phenolic compounds in the bio-oil [12]. EFB had the lowest lignin content (10.23 mass %) and the highest content of cellulose (44.97 mass %).

The total amount of extractives and the percentage distribution of them are shown in Table 2.4. Shell had the lowest extractives content (7.1 %) while fiber and EFB had similar

amounts of extractives (19.3%). The maximum amount of extractives for EFB and fiber were obtained during the ethanol-toluene extraction (Table 2.4).

3.2 Thermogravimetric and DSC analyses

3.2.1 Analysis of Raw Samples

Good agreement occurred between DTG and DSC curves for the three types of biomass. TG, DTG and DSC curves for shell, fiber and EFB are shown in Figure 2.1. DTG curves had two peaks for shell and fiber, and one peak for EFB. The DSC curves always had an additional peak at temperatures higher than 400 ^{o}C for shell and fiber (Figure 2.1).

The two DTG peaks for shell and fiber were similar to results obtained by Guo and Lua [2, 18] who worked with oil palm shell and fiber. The two peaks in fiber and shell indicate that the decomposition occurs in two steps. These reaction steps have been commonly assigned to hemicellulose and cellulose decomposition respectively [21]. The first step ranged from temperatures T_1 to T_2 with a maximum rate of decomposition at T_{max1} and the second step ranged from T_2 to T_3 with a peak at T_{max2} (Table 2.5).

In contrast both DTG and DSC of EFB (Fig. 2.1c) showed a single peak with a maximum rate of conversion at 301.5 °C. The maximum rate of decomposition was located between the two peaks presented for shell and fiber. In the case of EFB, neither the temperature corresponding to the maximum conversion rate nor the kinetic parameters estimated could be related to the main biomass components.

Solid state reactions are relatively slow compared to gas or solution reactions because molecular movement and collision do not usually control reactions in the solid state. Therefore, the reactions represented in TG and DSC analyses may be seen to occupy a wide span of temperatures [13, 14]. To obtain kinetic parameters using TG analysis, it is necessary to identify

points where the compounds begin to decompose (T_i) and the point when the reaction is complete (T_f). The selection of T_i and T_f in both cases is sometimes difficult to pin-point precisely [13, 14].

Gaur and Reed [12] stated that hemicellulose degradation occurs between 200 and 350°C. They showed that the maximum rate of degradation in a typical DTG hemicellulose curve occurred at 269 °C (heating rate of 10ºC min $^{-1}$). In a typical DTG curve for cellulose (Avicel) degradation starts above 320 °C; with a peak at around 340 °C (heating rate of 10ºC min $^{-1}$). Finally, these authors [12] state that lignin had a flat endothermic peak at 425 °C. This value is close to the maximum DSC value during the third peak in shell and fiber (423 and 420 °C respectively).

Grønli et al. [22] showed that small sample size is important with TG measurements. Large samples can have temperature gradient that could affect the measurements. Other authors [17] suggest that the observed phenomenon is only important for samples with a high heat of reaction such as cellulose. In order to verify the impact of sample size in palm oil byproduct samples, we conducted a test with different sample sizes. Figure 2.2 shows TG and DTG curves for shell (particles sizes between 2 and 2.8 mm) with sample sizes from 4.18 to 35.94 mg. Peak temperatures do not show any specific trend based on sample size. The small variability of the curves seen would correspond to the different composition of the shell themselves. This result agreed with the analysis showed by Stenseng et al. [17] working with wheat straw with samples sizes of 2, 5, 10 and 20 mg.

TG curves for shell particle size less than 0.5 mm showed a higher conversion ratio reflected in a residual mass around 27% compared with a 33% obtained in the sample with particle size 2 - 2.8 mm (Figure 2.3). The pyrolysis of small particles (< 2mm) is related to the

reaction temperature hence it is pure reaction kinetic controlled process [2] In particle sizes larger than 2 mm, pyrolysis is controlled not only by chemical reactions but also by heat transfer process. These particles present a more tortuous path for the volatile matter to be released allowing carbon deposition on porous surface increasing the final residue [2]. Observed changes could also be explained due to changes in chemical composition between samples < 0.5 mm and 2 – 2.8 mm. Shell samples with diameters larger than 2 mm have higher carbon contents (Table 2.1) suggesting the presence of larger amounts of lignin in that fraction. The concentration of Al, Fe, Ni, and Cu were higher in the shell < 0.5 mm (Table 2.2). Some of these metals could have certain catalytic effect contributing to the formation of large amounts of char.

3.2.2 Analysis of Extractives and Extractives Free samples

The presence of extractives and metals in raw biomass can modify considerably the thermal behavior of cellulose, hemicellulose and lignin. In order to estimate this influence, samples free of extractive were studied using TG. Soluble metals like potassium and sodium are also leached during the removal of extractives. These metals are known to have catalytic effects during biomass thermal degradation reactions. The thermal behavior of extractive fractions obtained using ethanol- toluene, ethanol and water, and the extractive free samples are presented in Figure 2.4.

The thermal behavior of extractives (DTG curves) cannot be described by a single degradation pattern due to the diversity in their chemical composition. However, it is possible to establish the existence of two clearly defined zones. The first zone corresponds to the evaporation of relatively low molecular weight compounds (temperatures up to 350 ^{o}C). The second zone corresponds to the cracking of large molecular weight extractive compounds (temperatures higher than 350 ^{o}C). This second zone seems to be especially important in the

ethanol-toluene extractives obtained from fibers and EFB. The results suggest the existence of larger amounts of heavy compounds in fiber and EFB fresh extracts or that these extractives have high tendency to react forming heavy compounds during or after extraction.

Extractive free samples show however two clear peaks for all the samples. The change in the shape of DTG curves is dramatic in the case of EFB (Figures 2.1c and 2.4d). This result indicates that some metals or organic compounds removed during extraction interfere with the thermal behavior of cellulose, hemicellulose or lignin. Stenseng et al. [17] reported a single peak in a wheat straw DTG curve with a heating rate of 40 °C min^{-1}. When they [17] washed the wheat straw, the DTG curve was split into two. They explained that behavior as resulting from removal of salts during washing and removal of significant amounts of water-soluble material from the straw. K and other salts are reported to have catalytic effects on char formation reactions [17, 23]. The results seen in our study could also be related to the higher salt concentrations.

3.3 Kinetic Constants for Shell, Fiber, and EFB as received

The rate of the thermal decomposition reaction can be expressed as:

$$\frac{d\alpha}{dt} = Kf(\alpha) \tag{1}$$

where α is the fractional reaction at time t. The fractional reaction α expressed in terms of change in sample mass is given by the following equation

$$\alpha = \frac{(W_0 - W)}{(W_0 - W_f)} \tag{2}$$

where W_0, W, and W_f are the initial, actual and final mass of the sample during an experiment, respectively.

f(α) is a function that is characteristic of the way the reaction interface occurs through the sample, and *K* is the reaction rate constant [24]. By analogy with the Arrhenius' law applied to gas phase processed by the collision theory of reaction rate [25] , *K* is expressed as follows

$$K = Ae^{-E/RT} \tag{3}$$

where *E*, the activation energy in KJ mol^{-1} is the barrier which must be surmounted during transformation of reactants into products, *A*, the frequency factor in s^{-1}, *R* is the gas constant, 8.314 kJ $kmol^{-1}K^{-1}$, and *T* is the absolute temperature in K [25]. Due to a lack of theoretical justification in applying Arrhenius' law to thermal solid decomposition, some authors [12] recommend the use of terms, "pre-exponential factor" and "exponent term" for *A* and *E,* respectively.

Combining Eq.1 and 3 for the non-isothermal conditions with a constant heating rate *β*, the following integrated equation can be obtained:

$$g(\alpha) = \int_0^{\alpha} \frac{d\alpha}{f(\alpha(} = \frac{A}{\beta}\int_0^{T} e^{(-E/RT)}dT \tag{4}$$

The right side of Equation (4) can be expressed as an asymptotic series as shown in Equation (5)

$$g(\alpha) = ART^2\left(1 - 2RT/E\right)e^{(-E/RT)}/\beta E \tag{5}$$

Twelve empirical alpha functions with their corresponding *g(α)* functions used in biomass decomposition studies have been reported in the literature [2, 26]. Gaur and Reed [12] have reported several mathematical methods to determine the kinetic parameters from the TG-experimental data. In this paper the method reported by Guo and Lua [18] was used taking into account the alpha functions given by Reading et al. [26].

To estimate the kinetic parameters ln $g(\alpha)/T^2$ is plotted versus $1/T$ (k^{-1}) (Equation 5) to give a straight line with a slope $-E/R$ and intercept of ln $AR/\beta E$ (Figure 2.6). The values of *E*

and *A* obtained by these means were compared for different *f(α)* to find the best linear correlation coefficient. To select the initial temperatures (T_i) and final temperatures (T_f) for each step, TGA and DSC curves were considered together. In Table 2.5, T1 was the average from the DSC curves when there was a suddenly heat flow increment. Tmax1, T2, and Tmax2, for shell and fiber were selected from the average of the maximum and minimum peaks from the TGA curves. T2 from EFB and T4 for shell and fiber were selected from the average temperature at the end of the last DSC peak.

In the low temperature regime (step 1), the pyrolysis model was based on a first order reaction ($f(\alpha)=1-\alpha$) for shell and fiber (Table 2.6). The *E* and *A* values for shell and fiber were 157 and 147 kJ mol $^{-1}$, and 4.1×10^{12} and 6.0×10^{12} respectively (Table 2.6). The second step had higher values of activation energy for both shell and fiber compared to the first step (Table 2.6). High activation energy indicates more difficulty of decomposition. The best mechanism obtained in the second step was also a first-order reaction. The activation energy for shell and fiber in the second step was around 229 kJ mol^{-1} (Table 2.6). That value is close to the activation energy reported for crystalline cellulose which ranges between 230 to 260 kJ mol^{-1} [12]. The frequency factor for shell and fiber in the second step were 5.3×10^{17} and 6.2×10^{17} s^{-1}, respectively. The model that fits best in the third step for shell and fiber was a two-dimensional model ($f(\alpha) = \left[-\ln(1-\alpha)\right]^{-1}$) (Table 2.6). The *E* and *A* values for shell and fiber using a two-dimensional model were 36.5 and 52.8 kJ mol^{-1}, and 1.3×10^{0} and 4.9×10^{1} s^{-1}, respectively. The *E* and *A* values obtained for EFB in a single step were 100.3 kJ mol $^{-1}$ and 1.06×10^{7} s^{-1}, respectively (Table 2.6).

3.4 Kinetic Analysis of Extractive Free Samples

The resulting DTG curves of extractives free samples can usually be described as the additive contribution of each of the samples polymeric constituents (cellulose, hemicellulose and lignin). These samples can be analyzed using the three independent reactions models. In these situations, the total thermal degradation rate of biomass can be assumed to be the sum of thermal degradation rates of its components. Here each component (cellulose, hemicellulose and lignin) proportionally contributes to the global degradation process. The equations generally used to describe the thermal decomposition of the individual species are:

$$\frac{d\alpha}{dt} = \sum_{j=1}^{N} z_{jo} \frac{d\alpha_j}{dt} \tag{6}$$

$$\frac{d\alpha_j}{dt} = A_j exp\left(-\frac{E_j}{R \times T}\right) \bullet (1-\alpha_j)^{n_j} \tag{7}$$

$$\sum_{j=1}^{N} z_{jo} = 1 \tag{8}$$

$$z_{jo} = \frac{(m_{jo} - m_{j\infty})}{(m_o - m_\infty)} \tag{9}$$

where:

$\frac{d\alpha}{dt}$: reaction rate.

$\frac{d\alpha_j}{dt}$: reaction rate for component j.

α_j : degree of conversion : $\alpha_j = \frac{(m_{jo} - m_j)}{(m_{jo} - m_{j\infty})}$

z_{jo} : mass fraction of volatile materials for component j.

A_j : pre-exponential factor corresponding to component j thermal degradation.

E_j : activation energy corresponding to component j thermal degradation.

m : mass of solid residue

n_j : reaction order

The kinetic parameters E_j, A_j, n_j, and z_{jo} that allow fitting the DTG curves are estimated using a least square regression method. The existence of 3 peaks, especially for EFB, became clearer (Figure 2.5) after adjusting the model. The first peak corresponds to hemicellulose, the second to cellulose and the third to lignin degradation. Table 2.7 summarizes the experimental values obtained for E_j, A_j, n_j and z_{jo} obtained for each of the extractive free samples. The kinetic parameters obtained by the first method and the ones obtained using the three independent models were plotted in a figure also containing other kinetic parameters reported in the literature for cellulose, hemicellulose and lignin [27] (Figure 2.7). The kinetic parameters obtained by the two methods fit well in the curve compared with the ones reported in the literature.

In order to determine the initial biomass composition (y_{jo}), it is necessary to use Equation 10. The maximum volatile matter yield that can be obtained for each isolated fraction must be known.

$$y_{jo} = \frac{z_{jo} \times X_{\infty}}{X_{j\infty}} \tag{10}$$

where:

y_{jo} : initial mass fraction of component j

z_{jo} : mass fraction of volatile material for component j

$X_{j\infty}$: maximum volatile yield corresponding to component j

X_{∞} : maximum volatile fraction, ($\frac{m_o - m_{\infty}}{m_o}$).

The biomass final conversion X_∞ and the final residue (R_s = 1- X_∞) can be determined experimentally (Table 2.7). By using Equation 11, the global volatile fraction can be computed:

$$X_\infty = \sum_{j=o}^{N} (y_{jo} \times X_{j\infty}) \tag{11}$$

The cellulose volatile yield has been reported to be between 92 and 97 mass % when the heating rate is in the range of 2 to 50 $^oC\ min^{-1}$ [28, 29]. The volatile yield of hemicellulose has been found to be between 75 and 79 mass % over the same range of heating rates [28, 30, 31]. The lignin volatile yield varies between 61 and 74 mass % depending on the nature of the lignin studied [32]. Here the volatile yields of cellulose, hemicellulose and lignin were considered to be: 92, 75 and 61 mass %, respectively.

The hemicellulose, cellulose, and lignin composition from the biomass calculated using Equation 10 are shown in Table 2.7 (Mass fraction of compounds). The results reported are not in agreement with the chemical composition determined in the first section (Table 2.3). The difference between the chemical composition obtained using the conventional characterization method using different reagents and the one obtained by thermogravimetry can be explained by the differences in the behavior of cellulose, hemicellulose and lignin bonds towards a chemical agent and during thermal treatment. The differences can be also explained due to the simplifications made in the three reactions model scheme like for example the assumption of no interaction between biomass constituents. In the method used it was also assumed that the thermal degradation of hemicellulose and lignin can be described by a single reaction step, however, some experimental evidences show that these two components have a significantly more complex behavior.

4. Conclusions

Chemical composition of the three palm oil mill residues was found to be different. EFB showed the highest moisture content and concentration of Na and K. Fiber obtained the highest concentration of Mg, Al, Ca and Fe. There were significant differences in the concentration of B, Al, Fe, and Cu between the two shell samples (2 - 2.8 mm and < 0.5 mm). Shell lignin content was higher than those in EFB and fiber.

Thermal behavior of shell (2-2.8 mm particle size) on DTG curves did not show any specific trend influenced by quantity of sample varied between 4.2 and 35.9 gm. The small variability of the curves would correspond to the different composition of the shells themselves.

The typical shell curve with particle size less than 0.5 mm showed a higher conversion ratio reflected in a weight loss around 27% compare with a 33% obtained in the sample with particle size 2 - 2.8 mm. A slower pyrolysis behavior, in shell 2 – 2.8 mm, was evident in the range 280 – 340 °C. This could be a result of heat transfer process alone that are more important in particles size between 2 – 2.8 than in particles less than 0.5mm. Another explanation could be the change in the chemical composition between the two samples.

Using DTG coupled with DSC analysis the thermal behavior of shell and fiber is explained as a three consecutive first order reactions. The E and A values for each step were related to the main biomass components e.g., hemicellulose, cellulose, and lignin. In contrast, degradation of EFB occurred in a single step. The change in the TG curve was evident for EFB raw samples and extractive free sample. A single peak was split in two when the extractives were removed. The high content of salts could have catalyzed the pyrolysis reactions. Kinetic parameters for cellulose, hemicellulose and lignin were obtained for the extractive free samples.

The composition of the biomass calculated using the three independent reactions model was not in agreement with the chemical composition determined by using the Ankor fiber analyzer. The variation can be explained by the differences in the behavior of cellulose, hemicellulose and lignin bonds towards a chemical agent and during thermal treatment. Another explanation could be the simplifying assumptions made such as lack of interactions between biomass constituents and single step transformation of individual constituents. Experimental evidences have showed that these individual components have a more complex behavior.

References

1. Corley, R.H.V. and P.B. Tinker, *The oil palm*. 4th ed. World agriculture series. 2003, Oxford ; Malden, MA: Blackwell Science. xxviii, 562 , [16] of plates.
2. Guo, J. and A.C. Lua, *Kinetic study on pyrolytic process of oil-palm solid waste using two-step consecutive reaction model.* Biomass and Bioenergy, 2001. **20**: p. 223-233.
3. Chen, G., J. Andries, and H. Spliethoff, *Catalytic pyrolysis of biomass for hydrogen rich fuel gas production.* Energy Conversion and Management, 2003. **44**: p. 2289 - 2296.
4. Yaman, S., *Pyrolysis of biomass to produce fuels and chemical feedstocks.* Energy Conversion and Management, 2004. **42**: p. 651 - 671.
5. Islam, M.N., R. Zailani, and F.N. Ani, *Pyrolytic oil from fluidised bed pyrolysis of oil palm shell and its characterisation.* Renewable Energy, 1999. **17**: p. 73-84.
6. Bridgwater, A.V. and J.L. Kuester, eds. *Research in thermochemical biomass conversion*. ed. E.a. science. 1988, Elsevier Science Publishers ltda.: Essex, England. 1193.
7. Bridgwater, A.V., ed. *Advances in Thermochemical Biomass Conversion*. Vol. 2. 1994, Blackie Academic & Professional: London. 1725.

8. Bridgwater, A.V., ed. *Pyrolysis and Gasification of Biomass and Waste*. 2003, CPL Press: Berks, U.K. 706.

9. Guo, J. and A.C. Lua, *Preparation of activated carbons from oil-palm-stone chars by microwave-induced carbon dioxide activation.* Carbon, 2000. **38**: p. 1985 - 1993.

10. Guo, J. and A.C. Lua, *Preparation and characterization of adsorbents from oil palm fruit solid wastes.* Journal of Oil Palm Research, 2000. **12**(1): p. 64 - 70.

11. Ani, F.N. and R. Zailani, *Characteristics of pyrolysis oil and char from oil palm shells*, in *Developments in thermochemical biomass conversion*, A.V. Bridgwater and D.G.B. Boocock, Editors. 1997: London. p. 425 - 432.

12. Gaur, S. and T.B. Reed, *Thermal Data for Natural and Synthetic Fuels.* 1998, New York: Marcel Dekker. 259.

13. Laye, P.G., *Differential Thermal Analysis and Differential Scanning Calorimetry*, in *Principles of Thermal Analysis and Calorimetry.*, P.J. Haines, Editor. 2002, The Royal Society of Chemistry: Cambridge, UK. p. 10 - 54.

14. Heal, G.R., *Thermogravimetry and Derivative Thermogravimetry*, in *Principles of Thermal Analysis and Calorimetry.*, P.J. Haines, Editor. 2002, The Royal Society of Chemistry: Cambridge, UK. p. 10 - 54.

15. Statheropoulos, M., et al., *Thermal degradation of Pinus halepensis pine-needles using various analytical methods.* Journal of Analytical and Applied Pyrolysis, 1997. **43**: p. 115 - 123.

16. Arvelakis, S., et al., *Prediction of the behaviour of biomass ash in fluidized bed combustors and gasifiers.* Journal of Thermal Analysis and Calorimetry, 1999. **56**: p. 1271 - 1278.

17. Stenseng, M., A. Jenses, and K. Dam-Johansen, *Investigation of biomass pyrolysis by thermogravimetric analysis and differential scanning calorimetry.* Journal of Analytical and Applied Pyrolysis, 2001. **58-59**: p. 765 - 780.

18. Guo, J. and A.C. Lua, *Kinetic study on pyrloysis of extracted oil palm fiber. Isothermal and non-isothermal conditions.* Journal of Thermal Analysis and Calorimetry, 2000. **59**: p. 763-774.

19. Caglar, A. and A. Demirbas, *Conversion of cotton cocoon shell to hydrogen rich gaseous products by pyrolys.* Energy Conversion and Management, 2001. **43**: p. 489-497.

20. Blanco Lopez, M.C., et al., *Composition of gases released during olive stones pyrolysis.* Journal of Analytical and Applied Pyrolysis, 2002. **65**(2): p. 313-322.

21. Williams, P.T. and S. Besler, *The pyrolysis of rice husks in a thermogravimetric analyzer and static batch reactor*. Fuel, 1993. **72**: p. 151 - 159

22. Gronli, M., M.J.J. Antal, and G. Varhegyi, *Round-robin study of cellulose pyrolysis kinetics by thermogravimetry.* Industrial and Engineering Chemistry Research, 1999. **38**(6): p. 2238-2244.

23. Fisher, T., et al., *Pyrolysis behavior and kinetics of biomass derived materials.* Journal of Analytical and Applied Pyrolysis, 2002. **62**: p. 331 - 349.

24. Gadalla, A.M., *Kinetics of dissociation of hydrated cerium (III) sulfate, nitrate and oxalate in air.* Thermochemica Acta, 1985. **95**: p. 179 - 200.

25. Bambford, C.H. and C.F.H. Tipper, eds. *Chemical Kinetics. Reaction in the Solid State.* 1980, Elselvier Scientific Publising Company: New York.

26. Reading, M., D. Dollimore, and R. Whitehead, *The measurement of meaningful kinetic parameters for solid state decomposition reactions.* Journal of Thermal Analysis, 1991. **37**: p. 2165 - 2188.

27. Garcia-Perez, M., *Co-pyrolysis under vacuum of bagasse and petroleum residue for the production of bio-fuels*, in *Chemical Engineering*. 2000, University of Laval. p. 110.

28. Varhegyi, G., et al., *Kinetic modeling of biomass pyrolysis.* Journal of Analytical and Applied Pyrolysis, 1997. **42**(1): p. 73-87.

29. Antal, J., Michael Jerry, G. Varhegyi, and E. Jakab, *Cellulose pyrolysis kinetics: Revisited.* Industrial & Engineering Chemistry Research, 1998. **37**(4): p. 1267-1275.

30. Di Blasi, C. and M. Lanzetta, *Intrinsic kinetics of isothermal xylan degradation in inert atmosphere.* Journal of Analytical and Applied Pyrolysis, 1997. **40-41**: p. 287-303.

31. Orfao, J.J.M., F.J.A. Antunes, and J.L. Figueiredo, *Pyrolysis kinetics of lignocellulosic materials - three independent reactions model.* Fuel, 1999. **78**(3): p. 349-358.

32. Jakab, E., O. Faix, and F. Till, *Thermal decomposition of milled wood lignins studied by thermogravimetry/mass spectrometry.* Journal of Analytical and Applied Pyrolysis, 1997. **40-41**: p. 171-186.

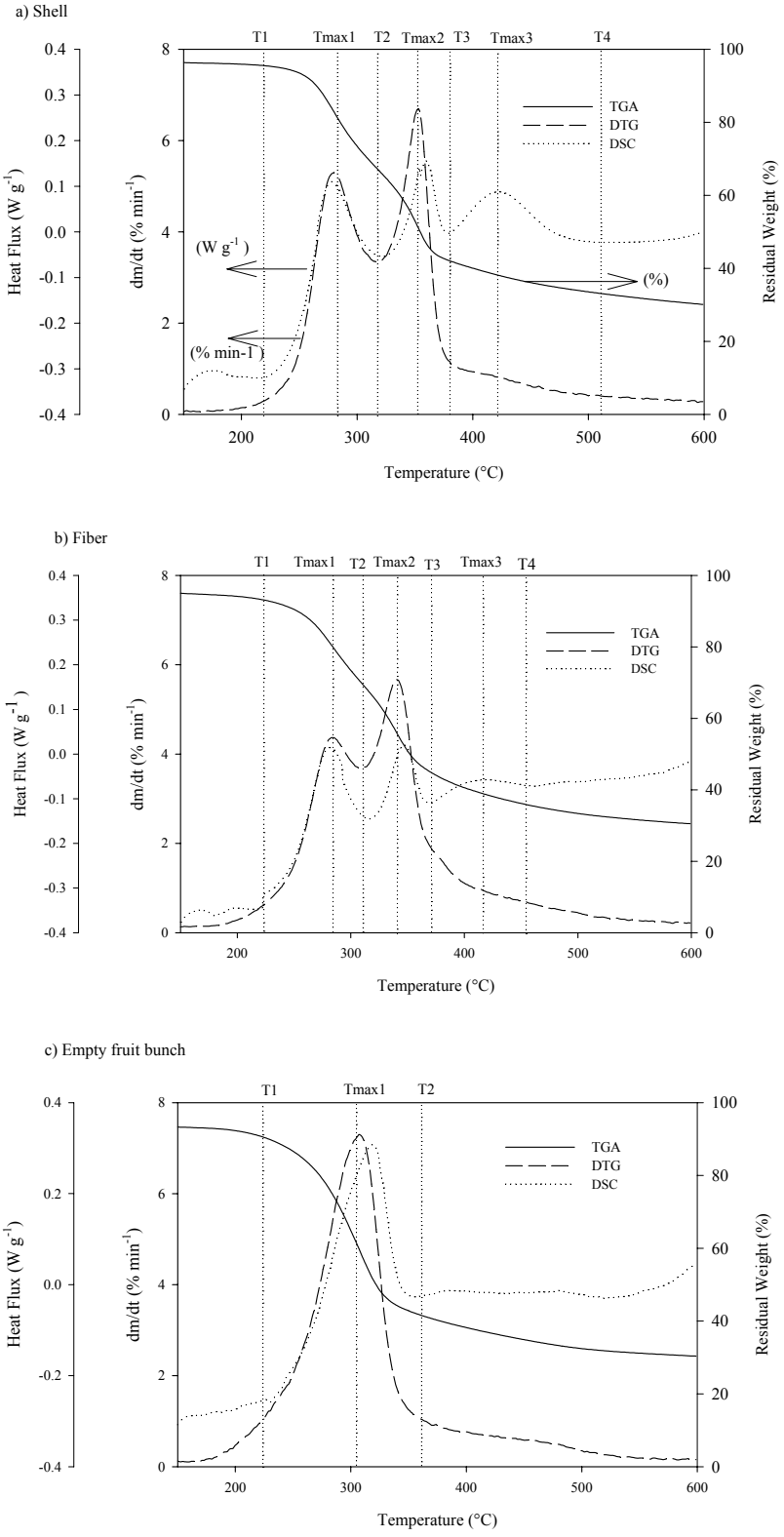

Figure 2.1 TG, DTG and DSC typical curves for shell, fiber, and empty fruit bunch at 10°C min^{-1}. The figures have the same scale coordinates in order to compare the data for different samples.

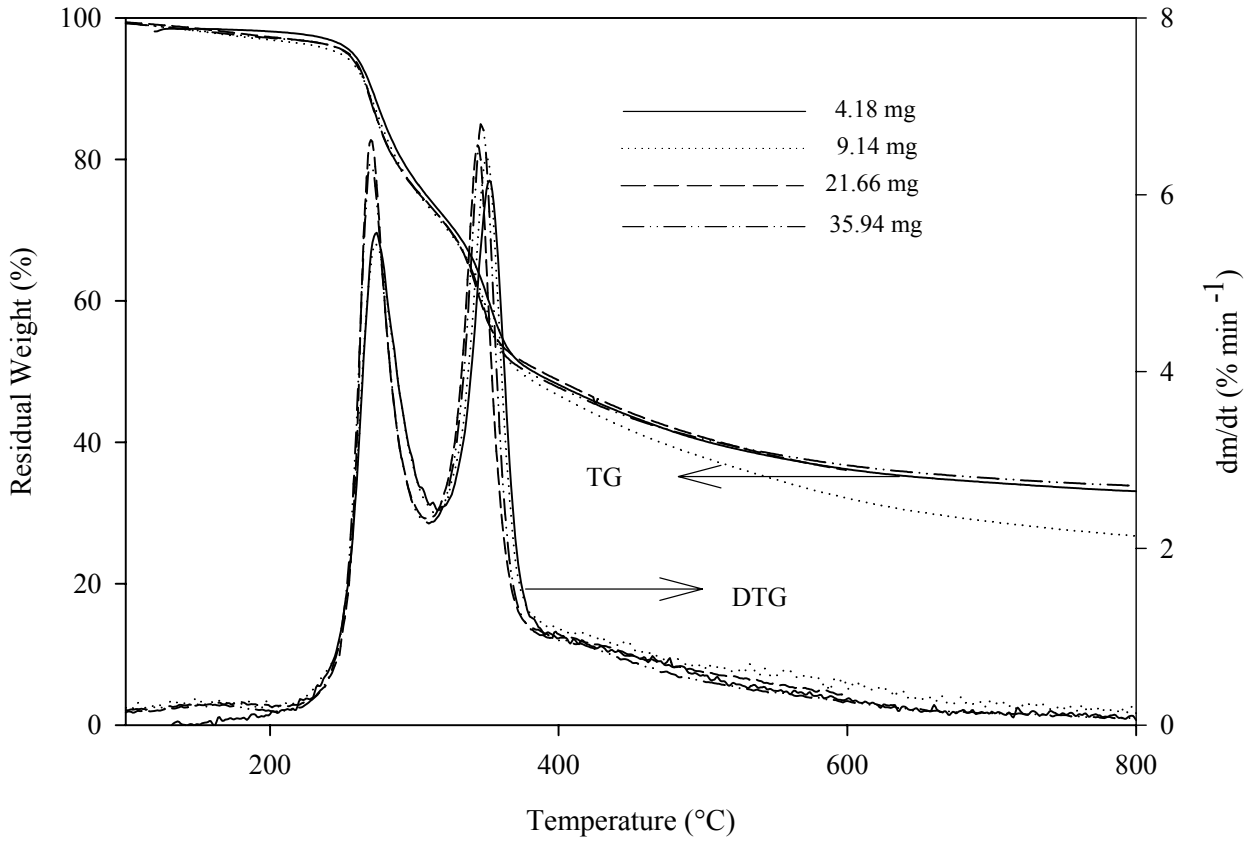

Figure 2.2 TG and DTG curves for shell > 2mm at 10 °C min^{-1} using different sample sizes. The name of each curve represents the sample weight in mg.

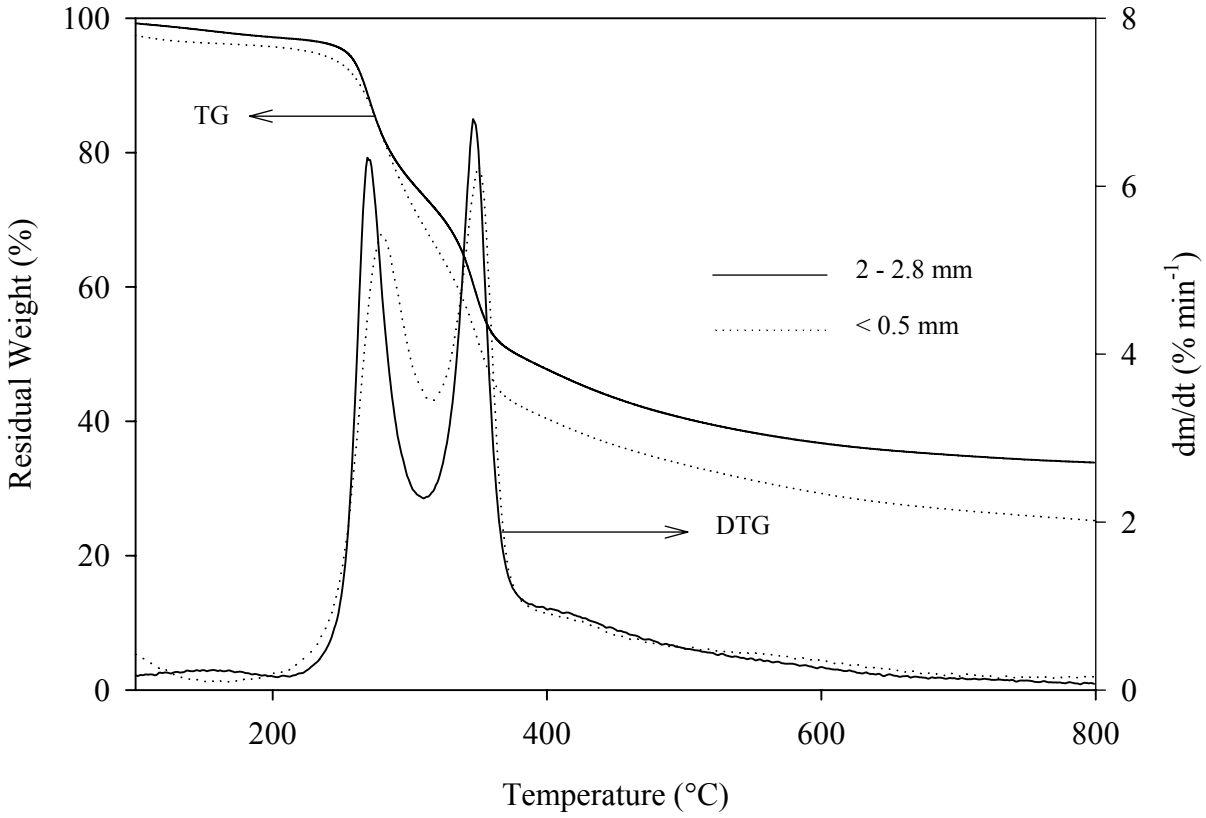

Figure 2.3 TG and DTG curves at 10°C min^{-1} for two different oil palm shell particles sizes.

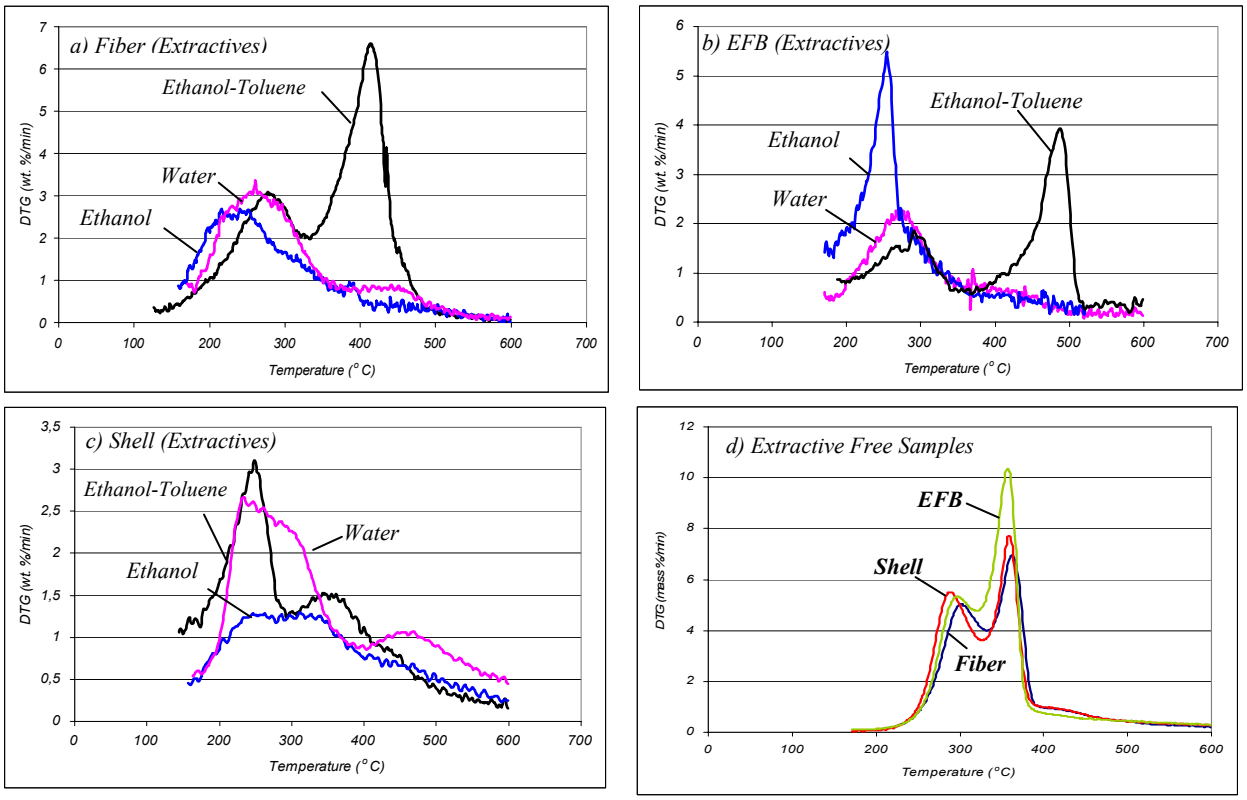

Figure 2.4 DTG curves of extractives and extractive free biomass.

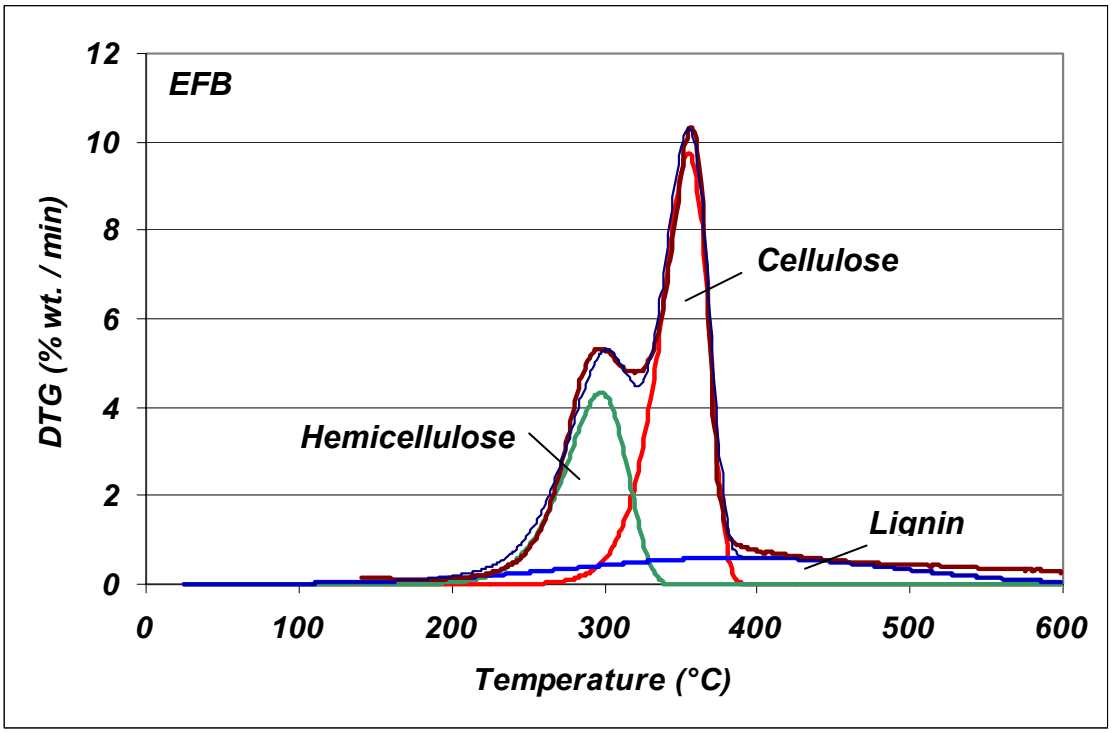

Figure 2.5 DTG curve of empty fruit bunch free of extractives at 10 ^{o}C min^{-1}.

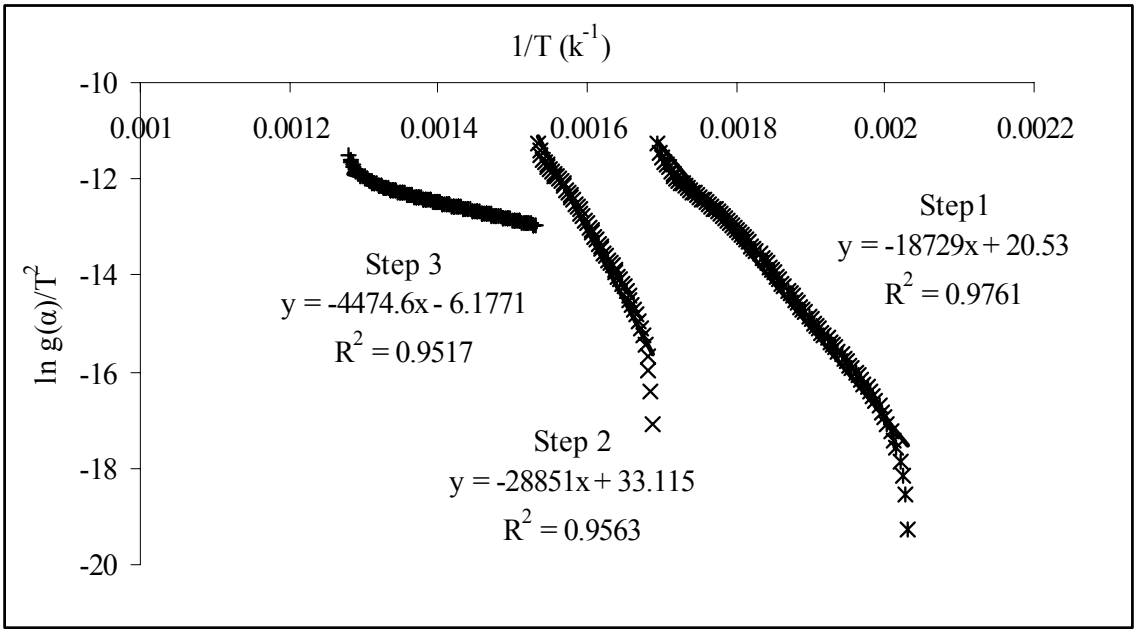

Figure 2.6 Graphical representation to obtain the values of *E* and *A* for one of the replicates for shell < 0.5 mm. The slope of each curve is equal to *–E/R*. The intercept is equal to ln *AR/βE*. For the first and second steps the best *f(α)* model was a liner model and for the third step the best *f(α)* function was a two dimensional model.

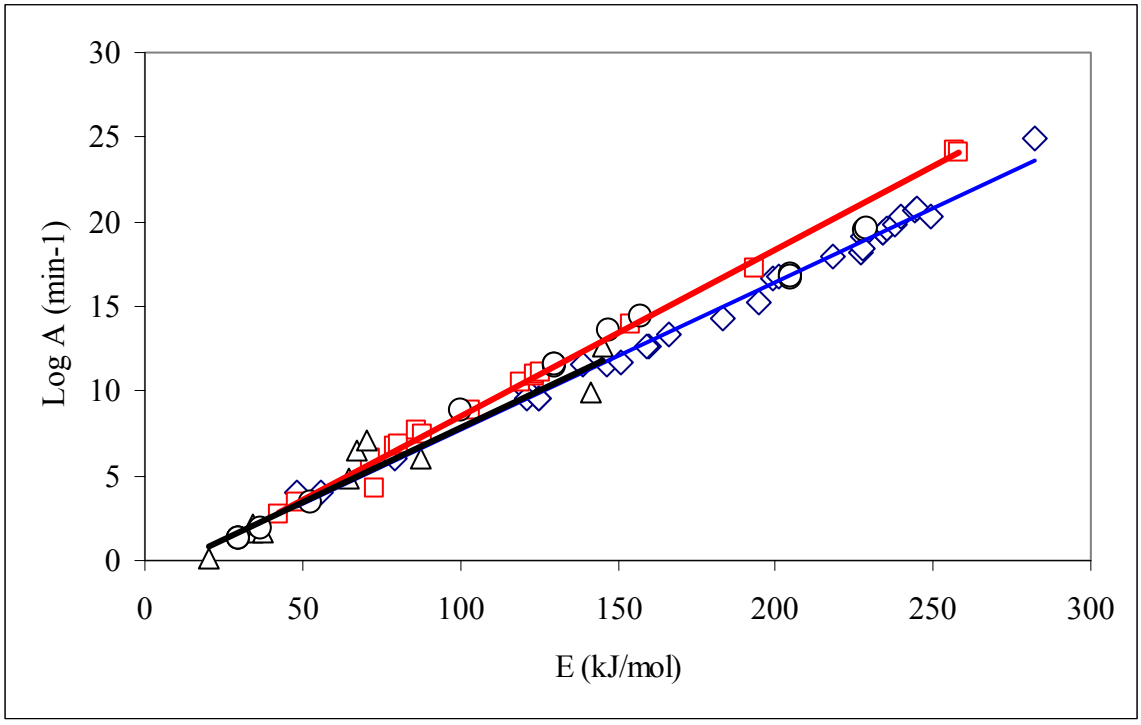

Figure 2.7 Thermal degradation kinetic parameters reported in the literature. ○ Values obtained in this paper ◇ for cellulose, □ for hemicellulose, △ for lignin.

Table 2.1 Percentage of C, N, S, moisture and ash in palm oil mill biomass

	Shell > 2mm	Shell < 0.5mm	EFB	Fiber
Moisture (%)	3.31	4.10	5.67	5.89
Ash [a] (%)	1.82 ± 0.34	2.02 ± 0.11	7.87 ± 0.30	8.44 ± 0.22
Volatiles at 600 ºC (%)	64.76 ± 2.12	70.65 ± 0.60	70.59 ± 2.05	69.39 ± 0.50
C (%)	49.61 ± 0.59	46.21 ± 3.16	40.88 ± 2.47	43.35 ± 2.28
N (%)	0.42 ± 0.03	0.36 ± 0.02	0.87 ± 0.09	1.21 ± 0.08
S (%)	0.06 ± 0.02	0.04 ± 0.00	0.09 ± 0.01	0.18 ± 0.02

[a] Dry free basis.

Table 2.2 Metals content (mg kg^{-1}) in palm oil mill biomass (three replicates per sample)

	Shell > 2mm	Shell < 0.5 mm	EFB	Fiber
B	13.45 ± 2.55	4.19 ± 0.87	15.79 ± 4.48	26.78 ± 3.45
Na	10.78 ± 3.02	13.33 ± 6.71	102.29 ± 16.02	32.87 ± 19.72
Mg	262.69 ± 10.29	250.65 ± 20.88	913.12 ± 264.97	1509.53 ± 180.22
Al	31.65 ± 9.02	336.48 ± 12.94	802.08 ± 263.65	1216.33 ± 133.75
P	115.04 ± 4.35	111.92 ± 15.47	572.70 ± 226.44	594.91 ± 68.08
K	1477.70 ± 58.84	1557.48 ± 98.34	22289.15 ± 2022.18	5188.26 ± 368.07
Ca	173.72 ± 10.77	160.84 ± 6.42	889.34 ± 290.96	1771.62 ± 104.34
Cr	1.52 ± 0.05	1.67 ± 0.07	2.68 ± 0.34	3.48 ± 0.14
Mn	15.82 ± 0.81	16.58 ± 1.60	83.67 ± 34.49	97.03 ± 9.72
Fe	56.25 ± 3.90	337.91 ± 32.78	812.35 ± 310.20	1239.39 ± 128.21
Ni	0.45 ± 0.15	1.17 ± 0.15	4.64 ± 1.78	2.76 ± 1.03
Cu	6.07 ± 0.52	16.11 ± 0.99	29.22 ± 10.61	37.31 ± 4.42
Zn	12.58 ± 3.60	11.35 ± 3.27	39.77 ± 20.80	27.18 ± 5.67
Se	0.14 ± 0.03	0.15 ± 0.04	0.30 ± 0.02	0.21 ± 0.03
Mo	0.09 ± 0.01	0.06 ± 0.01	0.10 ± 0.03	0.25 ± 0.01
Cd	0.01 ± 0.02	0.00 ± 0.01	0.09 ± 0.05	0.07 ± 0.05
Pb	17.31 ± 3.90	26.96 ± 5.52	9.78 ± 5.17	2.26 ± 0.13

Table 2.3 Cellulose, hemicellulose and lignin (acid detergent lignin) content (ash free) in defatted oil palm biomass samples.

	Lignin (%)	Cellulose (%)	Hemicellulose (%)
Shell	49.58 ± 0.15	30.28 ± 0.14	12.72 ± 0.05
EFB	10.23 ± 0.08	44.97 ± 0.44	19.92 ± 0.40
Fiber	21.79 ± 0.01	33.21 ± 0.02	16.58 ± 0.06

Table 2.4 Extractives in palm oil mill biomass.

	Ethanol-Toluene (%)	Ethanol (%)	Water (%)	Total (%)
Shell	4.14	0.66	1.29	7.13
EFB	11.90	1.16	6.26	19.32
Fiber	13.6	0.84	4.90	19.34

Table 2.5 Range of temperatures and temperatures of maximum mass loss for palm oil mill biomass during TG/DSC analyses.

	T1	Tmax1	T2	Tmax2	T3	Tmax3	T4
Shell	218.0	279.8	316.5	349.5	380.0	423.0	509.0
Fiber	222.0	283.5	310.0	341.5	369.0	419.5	457.0
EFB	172.0	301.5	361.0				

Table 2.6 Pyrolysis kinetic parameters for non-isothermal pyrolysis of oil palm biomass at 10°C min^{-1}. (Four replicates per sample)

Sample name	Weight	Step 1 (First order model)			Step 2 (First order model)			Step 3 (Two dimensional model)		
	(mg)	E kJ mol^{-1}	A s^{-1}	R^2	E kJ mol^{-1}	A s^{-1}	R^2	E kJ mol^{-1}	A s^{-1}	R^2
Shell	19.29	157.0	4.1E+12	97.7	228.2	5.3E+17	94.8	36.5	1.3E+00	93.9
S.D.	2.95	2.2	2.8E+12	0.2	16.7	5.1E+17	1.0	0.6	2.0E-01	1.2
Fiber	18.28	147.1	6.0E+11	96.9	229.0	6.2E+17	94.8	52.8	4.9E+01	92.5
S.D.	0.86	3.0	3.4E+11	0.2	7.3	9.6E+17	0.3	0.2	2.0E+0	3.6
EFB	19.17	100.3	1.1E+07	95.5						
S. D.	0.36	6.6	0.9E+06	1.5						

Table 2.7 Parameters used in the simulation of DTG curves of extractive free samples at 10 ^{o}C min^{-1}.

Component	*E (kJ/mol)*	*Log A (min-1)*	*n*	*Mass fraction of released Gases (z_{jo})*	*Mass Fraction of compounds (y_{jo})**
EMPTY FRUIT BUNCH (EFB) (mf=)					
Cellulose	205	16.84	1	0.51	0.40
Hemicellulose	130	11.58	1	0.29	0.28
Lignin	30	1.27	1	0.2	0.23
FIBRE					
Cellulose	205	16.64	1	0.37	0.30
Hemicellulose	130	11.43	1	0.31	0.32
Lignin	30	1.27	1	0.32	0.36
SHELL					
Cellulose	205	16.74	1	0.37	0.27
Hemicellulose	130	11.63	1	0.33	0.28
Lignin	30	1.27	1	0.30	0.35

*The difference to 100 % ash.

CHAPTER 3

PHYSICAL AND THERMAL MODELS OF PYROLYSIS OF OIL PALM SHELL IN A TUBULAR BENCH SCALE REACTOR [2]

[2] J.A. García-Núñez, K.C. Das, and T.M. Lawrence. 2005. To be submitted to *Biomass and Bioenergy*

Abstract

Pyrolysis of oil palm shell was achieved in an indirectly heated continuous flow reactor at target temperatures of 300, 350, 400, 500 and 600 ºC. A computer model using a set of equations that allows predicting temperatures and residual mass in different parts of the reactor was developed using the software Engineering Equation Solver (EES). The model was developed using differential scanning calorimetric (DSC) and thermogravimetric (TG) data coupled with energy and mass transfer equations. The model was calibrated using experimental data from 300, 400, and 600°C runs and was validated using independent data obtained at 350 and 500°C. The model predicted char yield at 350 and 500°C with an error less than 1.12 % compared to measured values. The model was used to predict the char production on oil palm fiber and oil palm empty fruit bunch (EFB).

Keywords: Oil palm biomass, pyrolysis, thermal model, oil palm shell, oil palm fiber, EFB, TG, DSC.

1. Introduction

Pyrolysis of biomass is the thermal degradation of the organic matrix in the absence of oxygen to obtain charcoal, bio-oil, and gases as products [1]. Pyrolysis has been used since ancient times not only for the production of charcoal but also for recovering distillation-products. Ancient Egyptians and Macedonians used pyrolysis for production of bio-oil and tar, production of charcoal [2]. At the end of the 19^{th} century and the beginning of the 20^{th} wood distillation was

a profitable industry for producing *"commercial products such as brown acetate of lime, grey acetate of lime, crystallized sodium acetate, "Iron liquor", and crude wood-naphtha"* [2]. With these materials, acetic acid, acetone, and methyl alcohol were obtained among other products [2, 3]. The advent of the petroleum industry caused a decline in the use of pyrolysis as a means of producing chemical compounds. Nowadays, because of energy and environmental concerns, pyrolysis of biomass is receiving increasing attention for production of pyrolytic liquid fuels, fuel gas, organic chemicals, and active carbon [4]. In a review paper, Yaman [1] reported more than one hundred biomass species which have been subjected to pyrolysis. In the last decades, pyrolysis has moved forward to find high valued products from bio-oil through fast pyrolysis [4-6].

One of the obstacles to widespread use of pyrolysis technologies is the availability, uniformity and cost of biomass [6-8]. In the case of the oil palm industry, large amounts of biomass are available at a single point, the palm oil mill (POM). One of the main solid residues produced by a POM is oil palm shell that is the endocarp of the fruits. The potential use of this large amount of biomass located in a single point, and the synergies of having a pyrolysis unit coupled with existing infrastructure, represents an opportunity for improving the conversion process in a POM.

Differential scanning calorimetry (DSC) and thermogravimetric analyses (TG) have been extensively used to study biomass pyrolysis process [1, 9]. TG is a method by which the mass change of a sample is recorded against temperature or time under controlled heating rate and inert gas atmosphere. DSC measures the amount of energy (heat) absorbed or released by a sample as it is heated, cooled, or held at a constant temperature, providing information of

endothermic (heat absorption) and exothermic (heat evolution) processes. It is used for the measurement and characterization of thermal properties of materials [9].

Combined thermal analysis using DSC/TG techniques in the biomass area has been explored in the past. Statheropoulos et al. [10] studied the thermal degradation of *Pinus halepensis*, forest species in the Mediterranean region. They correlated DSC and DTG curves to identify the compounds that have reacted at different temperatures. There was a good agreement between the two methods in identifying the temperatures at which the reactions occur. Arvelakis et al. [11] used DSC/TG curves to compare the thermal behavior of olive residue ash samples and leached olive residue ash samples. DSC and TG curves were in agreement in identifying the change in thermal behavior of the two kinds of samples. Stenseng et al. [12] used different sample masses of cellulose, wheat straw, and washed wheat straw in a simultaneous TG/DSC-system. A model which includes convection and radiations equations for the TG/DSC-system was developed to simulate the effect of sample mass.

Although quite powerful, the combination of DSC, TG, and heat transfer equations for modeling biomass pyrolysis has not been reported in the literature. In both DSC and TG analyses, a small sample of biomass (around 10 mg) is pyrolysed in an ideal condition. There are no restrictions to heat transfer, the interactions with the surroundings are controlled, and the heating rate and the carrier gas flows are controlled as well. In a bench scale reactor, the situation is far from ideal. The particles are interacting with each other in the bulk flow, the heating rate changes as the biomass moves from the cooled part to the heated area, and the energy exchange between the sample and the surroundings are changing constantly. This paper presents an approach to combine information from TG/DSC analyses with heat transfer

equations during pyrolysis of oil palm shell in an indirectly heated continuous-screw bench scale reactor.

2. Material and Methods

2.1 Samples

Oil palm shell used in these experiments was obtained from *Aceites S.A.* palm oil mill located on Colombian's north coastal region. The biomass was shipped from Colombia in plastic barrels to Athens, Georgia, USA and was stored at 4°C until processing. Shell was ground with a Fritsch laboratory cutting mill using a 2 mm trapezoidal perforations sieve cassette. The ground shell was dried for 24 hours at 105°C and stored in the plastic barrels before pyrolysis. Table 3.1 shows some typical chemical characterization of shell that have been reported in the literature [13-20].

2.2 Thermal analyses of samples

TG analysis of shell was conducted using a Mettler Toledo TG/SDTA851e. DSC analysis was carried out using a Mettler Toledo DSC821e. TG and DSC analyses were performed on shell samples after removing all impurities. Analyses conditions ranged between room temperature and 600°C at a heating rate of 10°C min^{-1} in an inert atmosphere by using nitrogen as carrier gas at a flow rate of 50 cm^3 min^{-1}. The shell particle size used for DSC and TG analyses ranged between 2.0 and 2.8 mm. Shell specific heat capacity, C_p, was determined using DSC curves by the direct method stated in User Com magazine [21] in the range 160º - 215 ºC. Shell bulk density was measured in triplicate by using a 500 ml graduated cylinder filled with sample and obtaining the dry weight of the sample.

2.3 Pyrolysis Reactor and Operation

Pyrolysis of the oil palm shell was conducted in an indirectly heated continuous flow reactor (Figure 3.1). The reactor consisted in a 100 mm diameter stainless steel tube (# 1, Fig. 3.1) placed in a Lindberg/Blue M (model: HTF55322A 1200°C) furnace (# 2). In the tube, an auger (#3) driven by a ¼ hp motor (# 4) was used to move the biomass through the tube. At one edge of the tube a 30 L hopper (# 5) coupled with a motor driven feeder (# 6) fed the biomass into the main auger reactor. Between the hopper and the furnace a cooling system (# 7) was placed to prevent excess heating of the tube near the hopper. The cooling system consisted of a 3 mm copper tube wrapped around the main tube in a 10 cm length. At the end of the tube, a stainless steel container (# 9) was placed to collect the charcoal. To prevent tar formation in the lines before the condensation set-up, thermal tapes were installed to keep the bio-oil vapors above 400 ºC. The vapors and the gases were passed through a vertical tubular condenser (# 10) and then to series of ice cooled collectors (# 11) to condense and trap the bio-oil vapors. A vacuum pump was used at the end of the set-up to keep a vapor flow through the reactor. Inert carrier gas (nitrogen) from a cylinder was supplied at three locations, the hopper (# N1), the main reactor (# N2) and the char container (# N3). Thermocouples were incorporated at different locations to monitor temperatures.

In the computer model the reactor was divided into 19 zones (Figure 3.2). Each zone was 5 cm long corresponding to one pitch in the auger. Thermocouples were located just before the cooling system (zone 2), after the cooling system (Zone 4), at the beginning of the heating element (zone 9) and at the end of the heating element (zone 14). Furnace temperature was measured just above zone 12.

In each experimental run, the equipment was heated in a nitrogen atmosphere until it reached steady-state conditions at the selected temperature. Shell biomass was fed from the hopper via the rotary valve at an approximate feed rate of 45 g min^{-1}. The average amount of biomass used in each run was 3.35 kg. The nitrogen flow rate was 4 L min^{-1} distributed as follow: 3 L min^{-1} into the main reactor (# N2), 0.5 L min^{-1} into the hopper (# N1), and 0.5 L min^{-1} into the char container (# N3). Different runs were conduced with furnace temperature maintained at 300, 350, 400, 500 or 600 ºC during operation. The auger speed was maintained between 1.56 and 1.76 rpm translating to a solid retention time of 6.8 to 7.8 min, between the heating zone and the char and vapor outlet (zone 9 – 19, Figure 3.2). The solid material that was deposited in the char collector was cooled at room temperature in an inert nitrogen environment.

2.4 Computer Model

2.4.1 Software

Engineering Equation Solver (EES) was used to implement the model. The software solves sets of algebraic and differential equations, and iteratively optimizes the solutions [22]. EES has two characteristics that make it a good choice for this application. The first is that EES solves all relevant equations simultaneously thus reducing the importance of the sequence of the equations, input variables, and constants in the equations. The second feature is that EES has a large built-in database of mathematical functions and thermophysical properties that help in calculations [22].

2.4.2 Governing equations

The model conceptually treats each zone as an independent reactor connected in series. Each zone is confined to a pitch inside the auger that receives and passes mass and energy

between adjacent reactors. In each zone, an overall energy balance equation was conducted (Figure 3.3) as shown below in Equation 1.

$$Q_{\text{heater i}} + Q_{\text{conduction i}} = Q_{\text{to zone i-1}} + Q_{\text{loss i}} + Q_{\text{sample i}} \quad (1)$$

$Q_{heater\ \text{i}}$ is the conduction heat input through the walls that comes in from the heater. It is only applied on the heating area (zones from 9 to 14) and is given using Equation 2. $Q_{conduction\ \text{i}}$ is the horizontal conduction heat input which comes in to zone *i*. It is used in all zones and always comes from the zone *i+1* to the zone *i* as it is given for Equation 3. $Q_{\text{to zone i-1}}$ is the heat which pass out from the *i* zone to the left-hand side *i-1* zone. It is used in all zones and is calculated using an equation similar to Equation 3. $Q_{\text{loss i}}$ is the external heat loss in the zone *i* and only applies to zones without heating elements. In zones with sleeves and insulation materials (zones 7, 8, 15, 16, 18, 19), $Q_{\text{loss i}}$ takes the form of a conduction heat loss through the isolation material. In zones 5, 6, and 17, $Q_{\text{loss i}}$ takes the form of heat loss due to convection processes.

$$Q_{\text{heater } i} = \left(T_{ow\,i} - T_i\right) \times 2\pi \times k_{\text{tube i}} \times \frac{L}{\ln\left(r_o / r_{mid}\right)} \quad (2)$$

$$Q_{conduction\ \text{i}} = k_{tube\ \text{i}} \times A_{conduction} \times \frac{\left(T_{i+1} - T_i\right)}{L} \quad (3)$$

Where

$T_{ow\,i}$: Outer wall temperature.

T_i : Temperature in the middle wall tube thickness in zone *i*.

$k_{\text{tube i}}$: Thermal conductivity of the stainless steel tube at a given temperature.

L: Pitch length.

r_o : Outer tube radius.

r_{mid} : Radius till the middle wall tube thickness.

$A_{conduction}$: Conduction area in the main tube between zones.

The term $Q_{sample\ i}$ in Eq. 1 involves the sample heat transfer in zone *i*. It includes both the heat due to the contact with the inner tube wall and the heat involved on the volatilization process, as shown in Equation 4. Both TG and DSC curves are involved in this equation with the DSC curve included in the heat of volatilization while TG used in the calculation of the average mass flux in zone *i* ($\dot{m}_{average\ i}$).

$$Q_{sample\ i} = \dot{m}_{average\ i} \times Cp_{biomass} \times \Delta T_{sample\ contac\ i} + \dot{m}_{average\ i} \times DSC_i \quad (4)$$

The initial and final sample temperatures in each zone, $T_{sample\ in\ i}$ and $T_{sample\ out\ i}$ respectively, have to be calculated to obtain the sample temperature change ($\Delta T_{sample\ contac\ i}$). In Equation 5 both these temperatures are related with the temperature in the middle wall tube thickness (T_i).

$$T_{sample\ out\ i} = T_{sample\ in\ i} + \eta \times \left(T_i - T_{sample\ in\ i}\right) \quad (5)$$

The efficiency factor η (Eq. 5) is a corrector factor that takes into consideration the efficiency of the equipment and other thermal effects that have not been explicitly accounted for the model. When η is equal to one, a maximum thermal efficiency is assumed and the sample temperature reaches the inner wall tube temperature in each zone. The actual value of η was determined by comparing results from the model with experimental results in a model calibration procedure. The η value which minimizes the mean square error (Equation 6) of the predicted

($Y_{estimated}$) versus the measured ($Y_{measured}$) char yield weight was selected for the model application.

$$MSE = \frac{\sum \left(Y_{estimated} - Y_{measured}\right)^2}{N} \quad (6)$$

2.4.3 Initial and boundary conditions

Information such as reactor radius, insulation material dimensions and auger speed were input to the EES program based on actual physical measurements in the equipment set-up. Specific heat and density of the biomass were input based on the measured values. Stainless steel thermal conductivities for different temperatures were obtained from the database in EES. Thermal conductivity of the insulation was given for a blanket-mineral fiber glass material. The air convection heat transfer coefficient inside the oven in zones 6 and 17 was set to be 9 W m^2 k^{-1} based on typical values of this coefficient for free convection gases [23].

The model was tested using the measured wall temperatures obtained during the runs at 300, 400, and 600 ºC. The unknown temperatures in some zones where calculated by interpolation between two known zones temperatures. Using the boundary conditions and TG and DSC data sets, EES solves for sample temperatures and residual mass in each zone. The model was validated using independent data (not used in calibration) comparing the estimated results from the model with the measured values of char yield for the runs at 350 and 500 ºC.

3. Results and Discussion

TG analyses of oil palm shell showed that the increment of weight loss started around 250 ºC. The residual weight at 600 ºC was around 30% of the initial mass (Figure 3.4). DSC showed three endothermic peaks around 260, 350, and 420ºC. Because TG curve uses a

small sample size and reactions occur under near ideal conditions, it can be considered as the minimum residual weight that can be reached at the analysis conditions.

The outer wall tube temperatures at the beginning and the end of the heating zones were measured during operation. Figure 3.5 shows the temperature profile in these two points for the run at 600 ºC. The outer wall temperature at the end of the heating area (zone 14, Figure 3.2) reached around 600 ºC and was constant during the pyrolysis time (Figure 3.5). The temperature at the beginning of the heating area (zone 9, Figure 3.2) reduced due to the cool biomass that was coming in. However it reached steady state conditions by the end of the pyrolysis time (Figure 3.5). Similar temperature behavior at the beginning and at the end of the heating zone was found for the runs at 400 and 500 ºC. However for the two cooler runs at 300 and 350 ºC there was larger variability (data not shown).

The char produced at 300 ºC was not completely carbonized and consisted of un-pyrolyzed materials. Work is ongoing to determine the chemical composition and the characterization of the char obtained at different temperatures.

The TG curve and the measured values were very close for temperatures greater than 400 ºC (Figure 3.6). However for the runs at 300 and 350 ºC they diverged from each other. It can be inferred that at higher temperatures the thermal stability of the equipment allows the shell to reach the maximum conversion into char. On the other hand, at lower temperatures, the equipment could not reach conditions required to convert all the potential biomass into char. This behavior could be reproducible using the model as it is shown in Figure 3.6. The η value found to test the model was 0.50 using the runs at 300, 400 and 600 ºC. With this value, the model was validated using the runs at 350 and 500 ºC. The root mean square error between the model and the measured data was 1.12%.

The model was used to predict the char production at different temperatures during pyrolysis of fiber and empty fruit bunches (EFB). TG and DSC analyses of fiber and EFB were carried out using the same procedure as for the shell. Density and specific heat values were measured as well for fiber and EFB. The corresponding thermal boundary conditions used during shell pyrolysis were used for predicting fiber and EFB char yield at a given temperature.

The model for fiber showed a similar pattern compare to shell pyrolysis. At temperatures around and greater of 400 ºC, the TG curve and the modeled curve showed small difference while in 350 ºC the predicted char yield was 57.9 % while the corresponding TG values was 50.8 % (Figure 3.7). At 300 ºC, the TG curve showed 73.4 % of char while the predicted value was 84%.

Char yield for EFB showed a different behavior compared to shell and fiber. The closeness between TG values and the predicted values started around 350 ºC (Figure 3.8) while in shell and fiber it started around 400 ºC. At 300 ºC the predicted char yield was 78.6% while the char yield from TG curve was 64.9%. It seems that the thermal model can predict the char production using the equipment setup for different kind of biomass. The char production will depend on both the biomass thermal characteristics (TG, DSC, Cp) and the general thermal efficiency of the equipment.

4. Conclusions and recommendations

The integration of TG and DSC analyses with energy and mass balances equations allowed development of a thermal model for predicting char yield during pyrolysis in an indirectly heated continuous flow reactor. The estimated values of char yield were closer to the measured values in the reactor than values obtained from TG curves.

At lower temperatures there was a gap between the TG curve and both char yield measured value and the modeled value. It was inferred that at low temperatures the equipment may not be able to supply the necessary heat to volatilize the biomass compounds thereby under-predicting the amount of char. On the other hand, at higher temperatures, the predicted char yield and the measured char yield were close to the values obtained from the TG curve. In these regimes there is an asymptotic behavior of the TG curve where further increase in temperature does not affect the mass loss greatly.

References

1. Yaman, S., *Pyrolysis of biomass to produce fuels and chemical feedstocks.* Energy Conversion and Management, 2004. **42**: p. 651 - 671.
2. Klar, M., *The Technology of Wood Destillation*. Second ed. 1925, London: Chapman & Hall Ltda. 496.
3. Lédé, J., M. Ferrer, and F. Broust, *Fast Pyrogasification and/or Pyroliquefaction of Biomass in a Cyclone Reactor*, in *Pyrolysis and Gasification of Biomass and Waste*, A.V. Bridgwater, Editor. 2003, CPL Press: Birmingham. UK. p. 706.
4. Vasalos, I.A., M.C. Samolada, and G.E. Achladas, *Biomass Pyrolysis for Maximizing Phenolic Liquids*, in *Research in thermochemical biomass conversion*, E.a. science, Editor. 1988, Elsevier Science Publishers ltda.: Essex, England. p. 241 -263.
5. Bridgwater, A.V., ed. *Advances in Thermochemical Biomass Conversion*. Vol. 2. 1994, Blackie Academic & Professional: London. 1725.

6. Sun, L., M. Xu, and R.F. Sun, *Behaviour of Corn Stalk in an Indirectly Heated Pyrolysis Reactor*, in *Pyrolysis and Gasification of Biomass and Waste*, A.V. Bridgwater, Editor. 2003, CPL, Press: Birmingham, UK. p. 706.

7. Grassi, G., *The European R&D Programme*, in *Research in Thermochemical Biomass Conversion*, A.V. Bridgwater and J.L. Kuester, Editors. 1988, Elsevier Science Publishers LTDA: New York, US.

8. Wan, E.I. and M.D. Fraser, *Economic Potential of Producing Liquid Tranportation Fuels From Biomass*, in *Research in Thermochemical Biomass Conversion*, A.V. Bridgwater and J.L. Kuester, Editors. 1988, Elsevier Science Publishers LTDA: New York, US.

9. Gaur, S. and T.B. Reed, *Thermal Data for Natural and Synthetic Fuels.* 1998, New York: Marcel Dekker. 259.

10. Statheropoulos, M., et al., *Thermal degradation of Pinus halepensis pine-needles using various analytical methods.* Journal of Analytical and Applied Pyrolysis, 1997. **43**: p. 115 - 123.

11. Arvelakis, S., et al., *Prediction of the behaviour of biomass ash in fluidized bed combustors and gasifiers.* Journal of Thermal Analysis and Calorimetry, 1999. **56**: p. 1271 - 1278.

12. Stenseng, M., A. Jenses, and K. Dam-Johansen, *Investigation of biomass pyrolysis by thermogravimetric analysis and differential scanning calorimetry.* Journal of Analytical and Applied Pyrolysis, 2001. **58-59**: p. 765 - 780.

13. Gomez, A., et al., *Transformacion termoquimica de la biomasa residual del proceso de extraccion de la palma de aceite: Tecnologias y perspectivas (Thermochemical*

transformation of the residual biomass from the palm oil extraction process: Technologies and prospects). Palmas (Colombia), 2004. **25.**(Especial): p. 388 -397.

14. Guo, J. and A.C. Lua, *Kinetic study on pyrloysis of extracted oil palm fiber. Isothermal and non-isothermal conditions.* Journal of Thermal Analysis and Calorimetry, 2000. **59**: p. 763-774.
15. Guo, J. and A.C. Lua, *Preparation and characterization of adsorbents from oil palm fruit solid wastes.* Journal of Oil Palm Research, 2000. **12**(1): p. 64 - 70.
16. Guo, J. and A.C. Lua, *Preparation of activated carbons from oil-palm-stone chars by microwave-induced carbon dioxide activation.* Carbon, 2000. **38**: p. 1985 - 1993.
17. Guo, J. and A.C. Lua, *Kinetic study on pyrolytic process of oil-palm solid waste using two-step consecutive reaction model.* Biomass and Bioenergy, 2001. **20**: p. 223-233.
18. Islam, M.N., R. Zailani, and F.N. Ani, *Pyrolytic oil from fluidised bed pyrolysis of oil palm shell and its characterisation.* Renewable Energy, 1999. **17**: p. 73-84.
19. Lua, A.C. and J. Guo, *Preparation and characterization of chars from oil palm waste.* Carbon, 1998. **36**(11): p. 1663 - 1670.
20. MD Kawser, J. and F.N. Ani, *Oil palm shell as a source of phenol.* Journal of Oil Palm Research, 2000. **12**(1): p. 86 - 94.
21. Metter Toledo, *Measuring specific heat capacity*, in *User*. 1988. p. 5.
22. F-Chart Software, *EES Engineering Equation Solver*. 2005.
23. Incoprera, F.P. and D.P. DeWitt, *Fundamentals of heat and mass transfer*. 5th ed ed. 2002, New York :. 981.

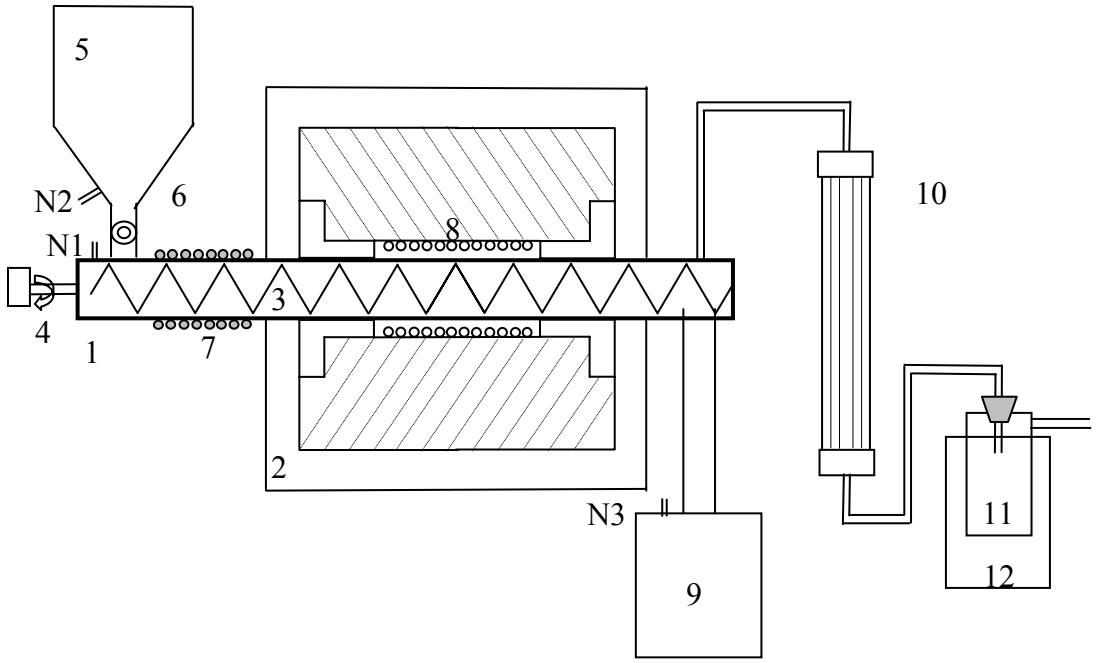

Figure 3.1 Schematic representation of the pyrolysis equipment set up. The equipment consists in the following components: 1- Main tube reactor. 2- Furnace. 3- Auger. 4- Motor to move the auger. 5- Hopper. 6- Feeder. 7- Cooling system. 8- Heating coil. 9- Char container. 10. Vertical tubular condenser. 11- Bio-oil traps. 12- Ice cooled containers. The nitrogen inlets are located in the following places: N1- Nitrogen inlet to the main reactor. N2- Nitrogen inlet to the hopper. N3- Nitrogen inlet to the char container.

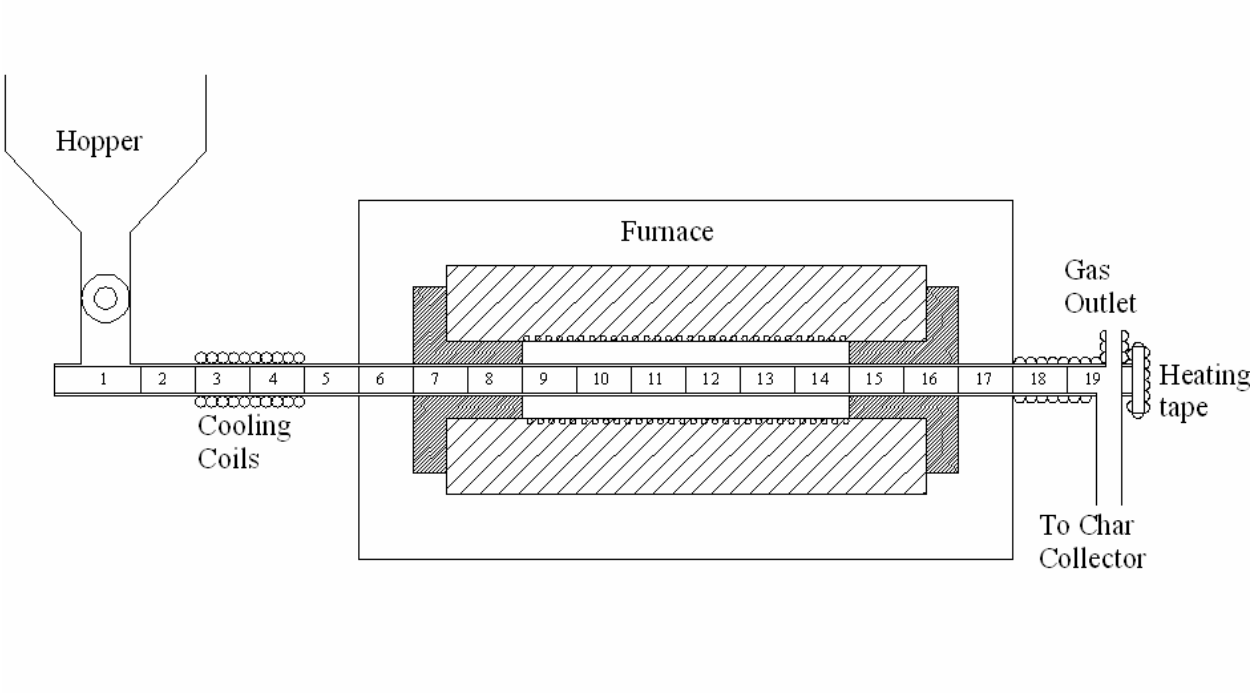

Figure 3.2 Schematic representation of the reactor dynamics in the computer model. Reactor length is divided into 19 computational zones with heated area between zones # 9 and zone # 14

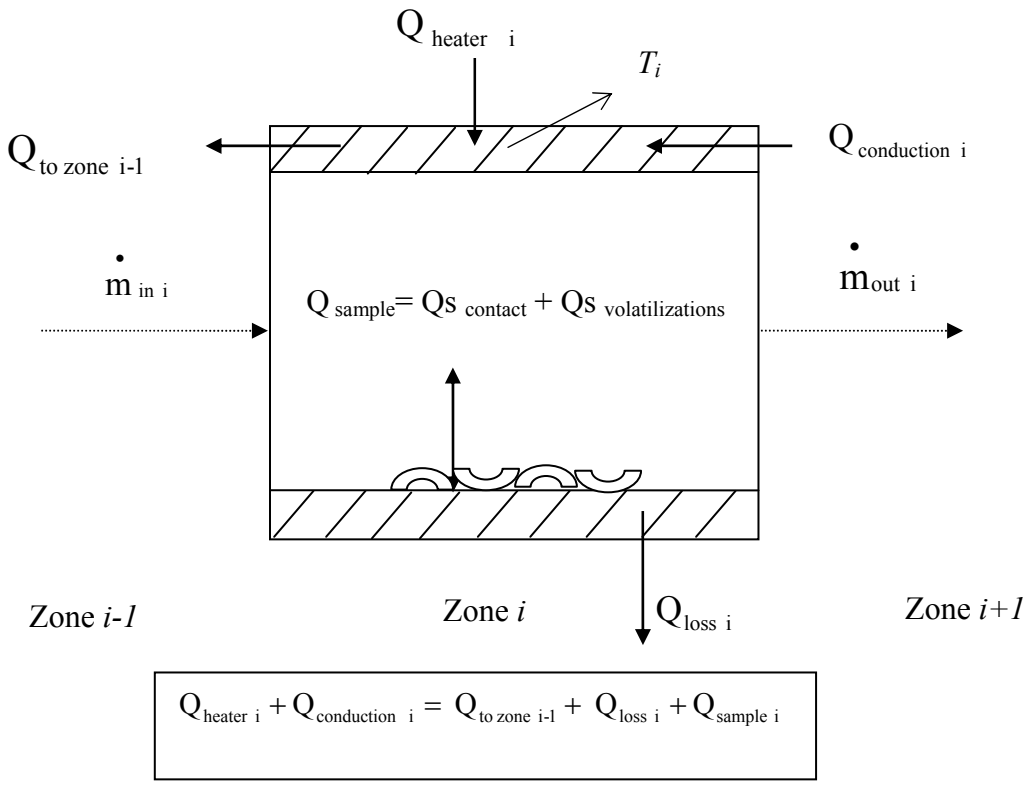

Figure 3.3. Schematic representation of the energy and mass balance in a zone *i*

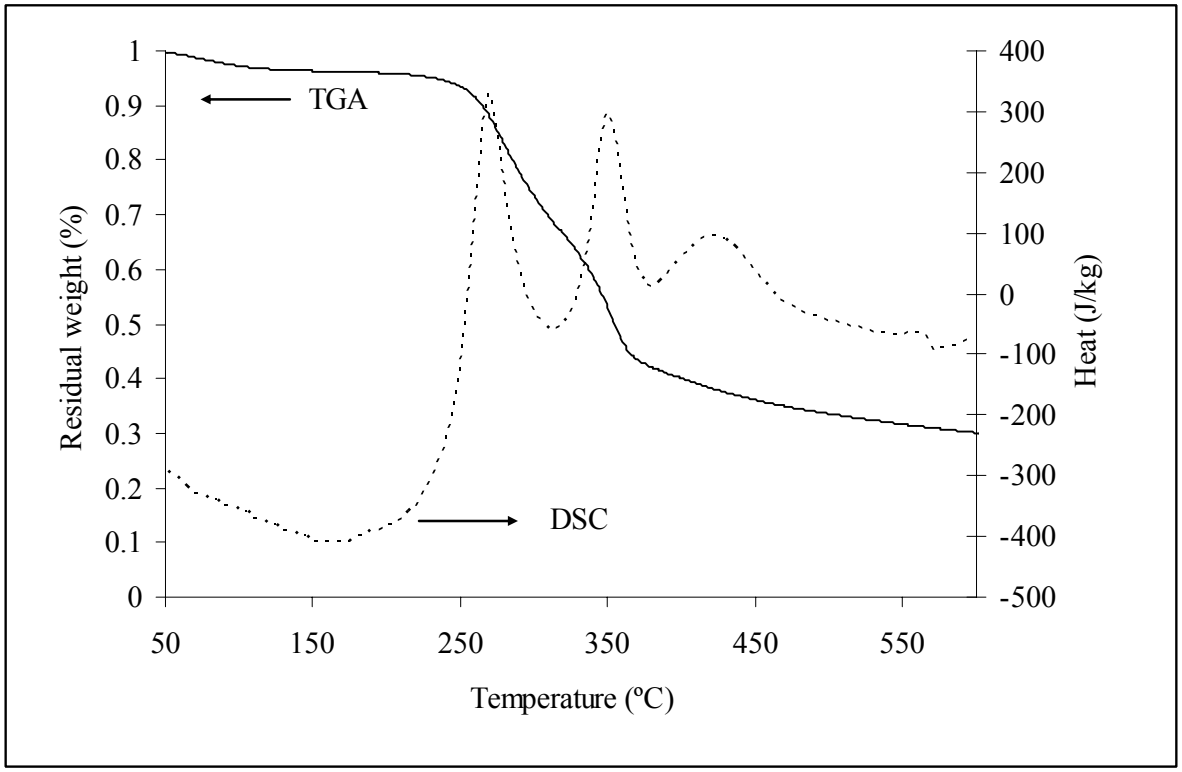

Figure 3.4 TG and DSC curves obtained from oil palm shell

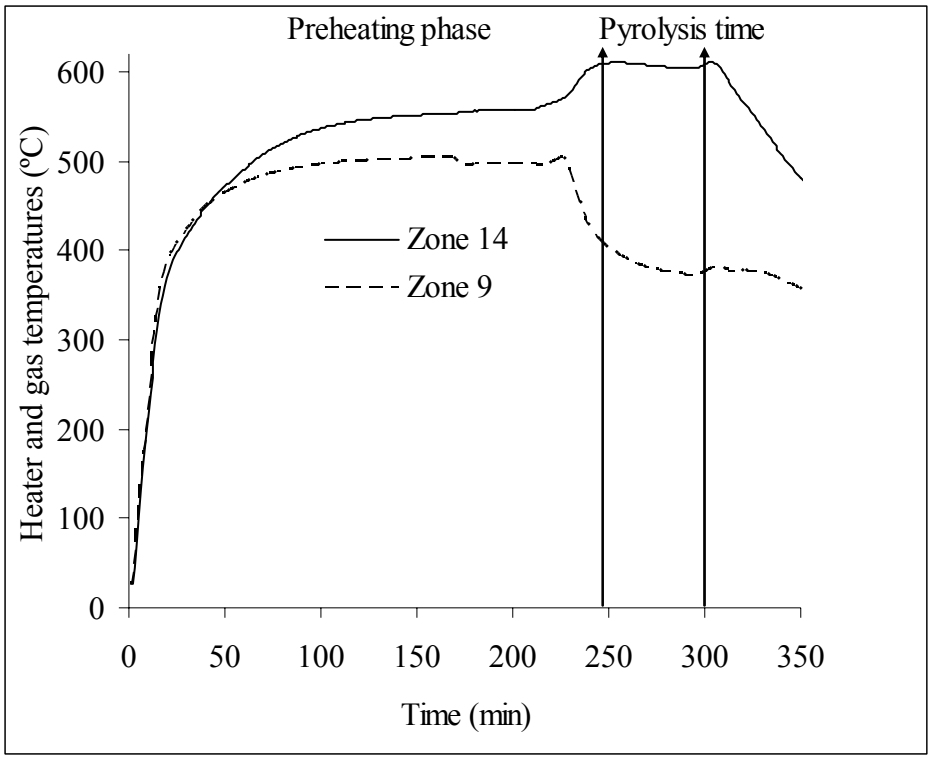

Figure 3.5 Outer tube temperature profile, at the beginning (zone 9) and at the end (zone 14) of the heating zone, in the pyrolysis of shell at 600 ºC

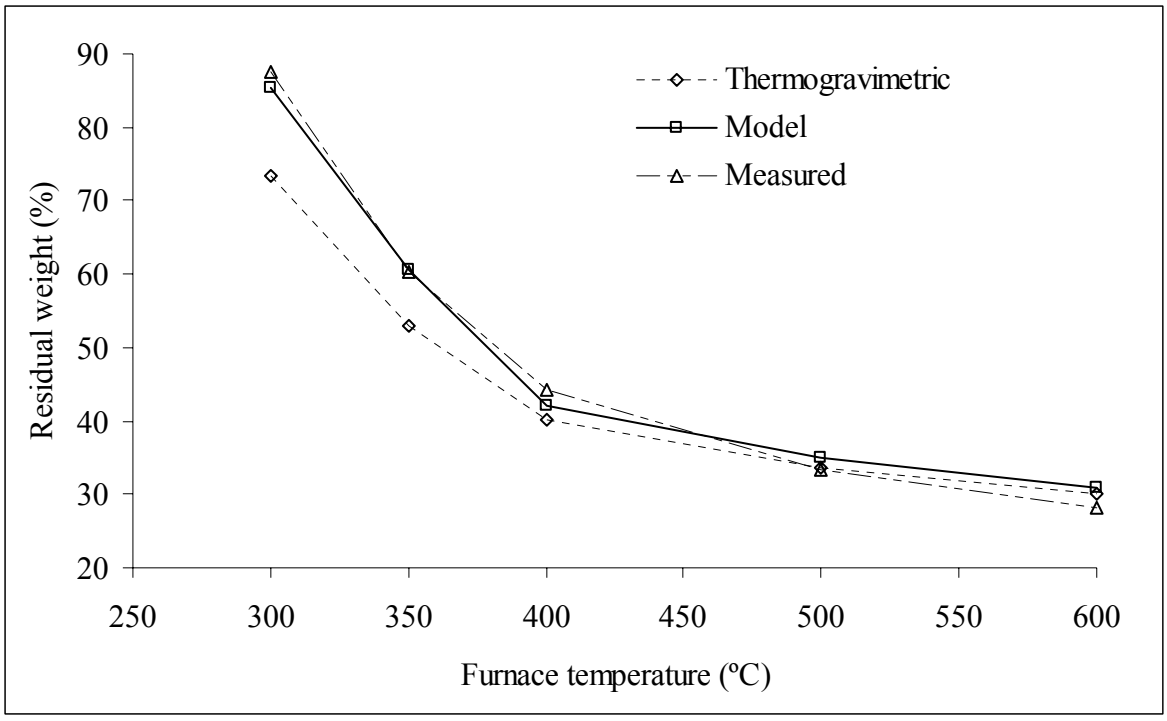

Figure 3.6 Comparison of char yield curves for pyrolysis of oil palm shell among thermogravimetric, measured data, and the information obtained with the thermal model. Data from runs at 350 and 500 ºC were used for validation.

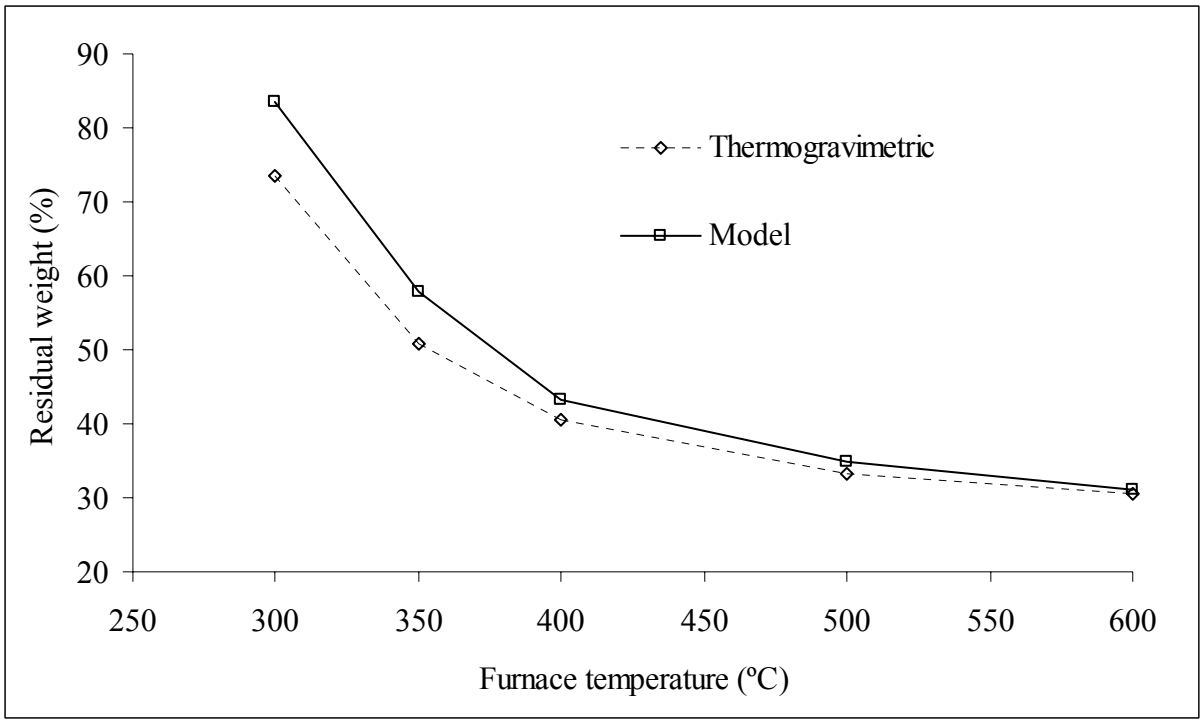

Figure 3.7 Simulation of char yield from fiber and corresponding thermogravimetric curve

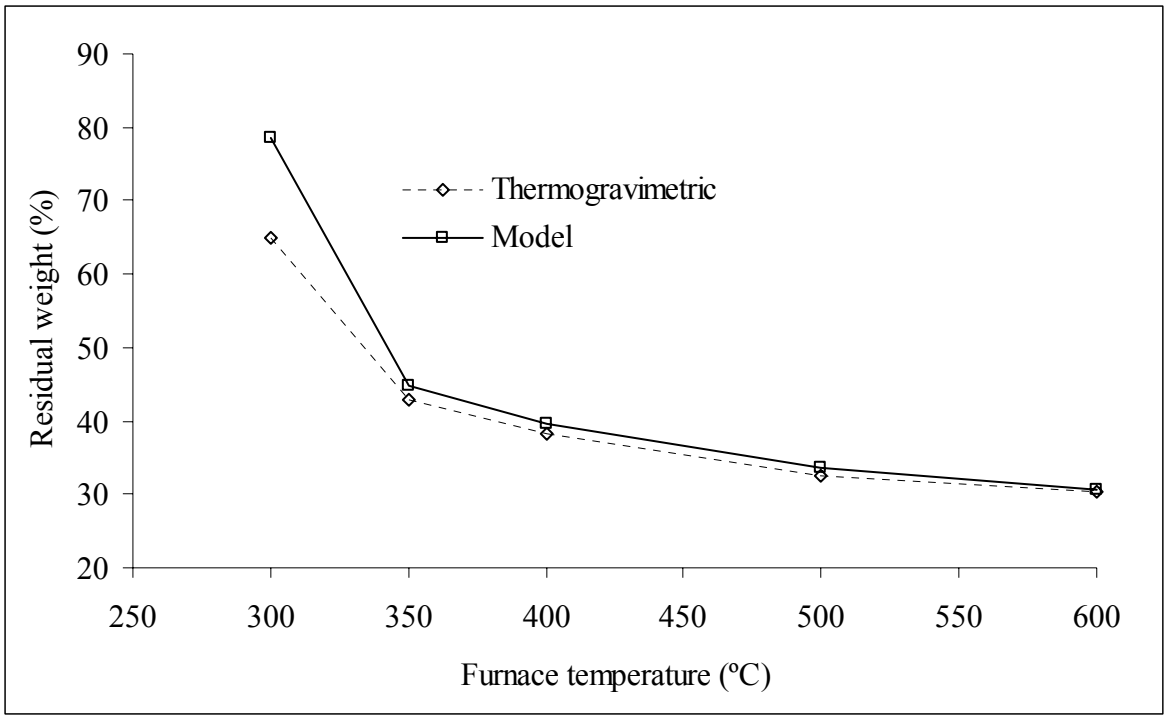

Figure 3.8 Simulation of char yield from EFB and corresponding thermogravimetric curve

Table 3.1 Elemental composition and proximate analysis of oil palm shell.

Elemental analysis	
Carbon (%)	52.5 - 55.4
Hydrogen (%)	5.7 - 6.4
Nitrogen (%)	0.37 - <1
Oxygen (%)	37.9 - 44.4
Proximate analysis	
Moisture (%)	8.40 - 11.2
Volatile matter (%)	68.9 - 80.8
Fixed Carbon (%)	17.3 - 20.4
Ash (%)	1.9 - 2.6
Gross calorific value ($MJkg^{-1}$)	19.10
Solid density (g/cm^3)	1.53
Apparent density (g/cm^3)	1.47
Total porosity (%)	3.9

Sources [13-20]

CHAPTER 4

CONCLUSIONS

A key contribution of this research is the use of TG/DTG analyses coupled with DSC analysis to obtain the kinetic constants of biomass degradation. Although DTG curves only showed two peaks indicating a two step process, the combination with DSC allowed us to explain the thermal behavior of shell and fiber as a three step consecutive process. The *E* and *A* values for each step were related to the main biomass components, namely hemicellulose, cellulose, and lignin.

Another contribution of this thesis was to report for the first time the thermal degradation of EFB. It was shown that the thermal degradation of EFF occurs in a single step using DSC and DTG analyses. However, when extractive free EFB samples were used, the DTG curve was split in two. It seems that the high content of salts and extractives could have catalyzed the pyrolysis reactions.

The composition of the biomass estimated using the three independent reactions model was different from the composition determined by chemical analysis using the Ankor fiber analyzer. This variation can be explained by the differences in the behavior of cellulose, hemicellulose and lignin bonds towards a chemical agent and during thermal treatment. Another explanation could be the simplifying assumptions made such as lack of interactions between biomass constituents and single step transformation of individual constituents.

Another important development was the integration of TG and DSC analyses with energy and mass balances equations to model char yield during the pyrolysis of oil palm shell in a

continuous flow reactor. This approach has practical implications of predicting the char production of a biomass at different temperatures by knowing the TG and DSC curves. Further opportunities exist in improving the model to predict oil production, quality of products, energy consumption, etc.